ÉCOLE POLYTECHNIQUE
FÉDÉRALE DE LAUSANNE

MATHICSE
Mathematics Institute of Computational Science and Engineering
School of Basic Sciences - Section of Mathematics

MATHICSE Technical Report
Nr. 09.2011
September 2011

Numerical approximation of internal discontinuity interface problems

Marco Discacciati, Alfio Quarteroni and Samuel Quinodoz

http://mathicse.epfl.ch

Phone: +41 21 69 32555

Address:
EPFL - SB - MATHICSE (Bâtiment MA)
Station 8 - CH-1015 - Lausanne - Switzerland

Fax: +41 21 69 32545

NUMERICAL APPROXIMATION OF INTERNAL DISCONTINUITY INTERFACE PROBLEMS

MARCO DISCACCIATI*, ALFIO QUARTERONI†, AND SAMUEL QUINODOZ‡

Abstract. This work focuses on the finite element discretization of boundary value problems whose solution features either a discontinuity or a discontinuous conormal derivative across an interface inside the computational domain. The interface is characterized via a level-set function. The discontinuities are accounted for by using suitable extension operators whose numerical implementation requires a very low computational effort. After carrying out the error analysis, numerical results to validate our approach are presented in one, two and three dimensions.

Key words. finite element, interface problem, level set

AMS subject classifications. 65N12, 65N30

1. Introduction. This paper is focused on the numerical approximation of elliptic problems whose solution features discontinuities across interfaces internal to the computational domain. We consider a Poisson problem in two disjoint subdomains of the computational domain $\Omega \subset \mathbb{R}^N$ $(N = 1, 2, 3)$ with jump conditions across the interface Γ separating the two subregions. Γ is a point if $N = 1$, a line if $N = 2$ or a surface if $N = 3$ that is characterized by a level-set function $\phi : \Omega \to \mathbb{R}$. We consider an open bounded domain Ω partitioned into the two non-overlapping subdomains $\Omega_1 = \{x \in \Omega |\ \phi(x) < 0\}$ and $\Omega_2 = \Omega \setminus \bar{\Omega}_1 = \{x \in \Omega |\ \phi(x) > 0\}$. See Fig. 1.1 for two possible instances. According to the classical level-set method (see, e.g., [17] and [24]), ϕ is regarded as the signed distance function to the interface, whence Γ is defined by the equation $\phi = 0$.

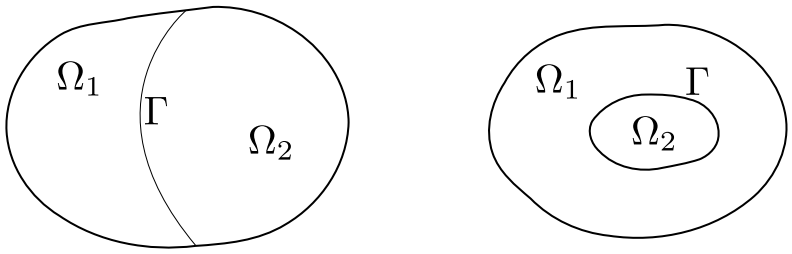

FIG. 1.1. *Two examples of partition of the domain* Ω.

The mathematical formulation of our problem is as follows. We look for a function u in Ω that satisfies a Poisson problem in each subdomain:

$$-\Delta u_i = f_i \quad \text{in } \Omega_i, \quad i = 1, 2, \tag{1.1}$$

*Laboratori de Càlcul Numèric (LaCàN), Escola Tècnica Superior d'Enginyers de Camins, Canals i Ports de Barcelona (ETSECCPB), Universitat Politècnica de Catalunya (UPC BarcelonaTech), Campus Nord UPC - C2, E-08034 Barcelona, Spain (marco.discacciati@upc.edu).

†MATHICSE, Chair of Modelling and Scientific Computing, Ecole Polytechnique Fédérale de Lausanne, Station 8, CH-1015 Lausanne, Switzerland. MOX, Politecnico di Milano, P.zza Leonardo da Vinci 32, I-20133 Milano, Italy (alfio.quarteroni@epfl.ch).

‡MATHICSE, Chair of Modelling and Scientific Computing, Ecole Polytechnique Fédérale de Lausanne, Station 8, CH-1015 Lausanne, Switzerland (samuel.quinodoz@epfl.ch).

where $u_i = u_{|\Omega_i}$, with the following conditions on the jumps of the trace and of the normal derivatives across Γ:

$$[\![u]\!]_\Gamma = u_{2|\Gamma} - u_{1|\Gamma} = g_d, \tag{1.2}$$

$$\left[\!\left[\frac{\partial u}{\partial n}\right]\!\right]_\Gamma = \nabla u_2 \cdot n_2|_\Gamma + \nabla u_1 \cdot n_1|_\Gamma = g_n. \tag{1.3}$$

g_d and g_n are two assigned functions on Γ, while n_1 and n_2 are the unit normal vectors on Γ directed outwards of Ω_1 and Ω_2, respectively. Notice that $n_2 = -n_1$ on Γ. We assume $f_i \in L^2(\Omega_i)$, $g_d \in H^{1/2}(\Gamma)$ and $g_n \in L^2(\Gamma)$. For simplicity, we impose homogeneous Dirichlet boundary conditions on the boundary of the domain Ω: $u = 0$ on $\partial\Omega$. Remark that if $\partial\Omega \cap \Gamma \neq \emptyset$ (see Fig. 1.1, left), then the compatibility condition $g_d|_{\partial\Omega\cap\Gamma} = 0$ must hold.

Discontinuities in the normal derivative of the solution of a PDE arise e.g. as soon as a force is localized on a part of the computational domain with lower dimension. The most popular example is the surface tension in flow simulations [18], a force that applies at the interface between two fluids. In this framework, Γ is a free surface, that is its location is a further unknown of the problem at hand. It can also happen that the solution itself is discontinuous, for example with phase transition when considering entropy [7] or with incompressible flames [16].

A possible strategy to correctly approximate this kind of problems is to build a mesh which captures the interface. This approach however may not be convenient. For instance, as for a time dependent problem, conforming meshes (that is meshes that perfectly match on the interface) have to be rebuilt at each time step, resulting in too expensive schemes in terms of computational cost. The mesh could also be cut by the interface and only locally rebuilt, but this could lead to highly deformed cells. Methods that do not require the reconstruction of a new mesh are in general preferable. For the same reasons, a good method should neither require mesh refinement near the interface, nor the computation of quantities (such as integrals) on the interface itself.

A method for solving problem (1.1) with a non-conforming mesh cannot rely on standard finite element discretization. Indeed, it has been shown in [10] that if a Lagrangian finite element space is used to approximate the solution, then one cannot expect a convergence rate better than $\sqrt{h}$ (h being the finite element grid size). This has been the main motivation for the development of new methods, such as XFEM [5] and a variant of Nitsche's method [11]. These methods share the same strategy: the finite element space is enriched with additional shape functions especially designed to resolve the discontinuities across the interface Γ. Even though they have been successfully applied to different kind of multiphysics problems (e.g. [2], [8] and [10]), still they are affected by some inherent weaknesses. The addition of these new shape functions can worsen the conditioning of the algebraic system and preconditioning strategies have to be redesigned for these methods (see e.g. [3]). Moreover, the parallel implementation of such methods might be troublesome when dealing with time dependent problems, as the number of degrees of freedom might vary while the interface is evolving.

The goal of this paper is to present a new method, called SESIC (standing for Simplified Exact Subgrid Interface Correction), that takes into account these jump conditions in a finite element framework. Our method has been inspired by the ESIC

method developed in [12]: we have improved the construction of the liftings and changed the weak formulation so that the efficiency of the ESIC is kept while improving its mathematical interpretation and its effective implementation. Indeed, in the SESIC method, no polynomial refinement is required in the interface zone to obtain optimal convergence and, under certain conditions, the interface does not need to be explicitly reconstructed. The paper has the following content. In section 2, we study the weak formulation of the internal discontinuity problem (1.1)-(1.3) and we introduce at the continuous level suitable lifting operators to account for the jumps across the interface. In section 3, we present the finite element approximation of the problem and discuss several numerical issues of our methodology in comparison with the one developed in [12]. In section 4 we provide an error analysis of our method in both H^1 and L^2 norms. Finally, in section 5 we illustrate the numerical results that we have obtained on different test cases.

2. Weak formulation for the internal discontinuity interface problem. To derive a weak formulation of (1.1) - (1.3), we introduce two suitable liftings (or extensions) $R_i g_d$ $(i = 1, 2)$ of g_d in Ω_i so that the jump of $R_i g_d$ is g_d on Γ: $R_i g_d \in H^1_{\partial\Omega_i \setminus \Gamma}(\Omega_i) = \{v \in H^1(\Omega_i) | v = 0 \text{ on } \partial\Omega_i \setminus \Gamma\}$ $(i = 1, 2)$ such that $[\![R_i g_d]\!]_\Gamma = g_d$. The trace theorem (see [15]) guarantees that such a lifting operator exists. Then, we consider the splitting

$$u_i = \bar{u}_i + R_i g_d \quad \text{in } \Omega_i. \tag{2.1}$$

We denote $\bar{u} : \Omega \to \mathbb{R}$ such that $\bar{u}_i = \bar{u}|_{\Omega_i}$. The function $\bar{u}$ belongs to $H^1_0(\Omega)$. We consider a global test function $v \in H^1_0(\Omega)$ and its restrictions v_i on Ω_i. Then, on each domain, starting from (1.1), integrating by parts and exploiting the homogeneous Dirichlet boundary conditions on $\partial\Omega_i \cap \partial\Omega$, we obtain

$$\int_{\Omega_i} \nabla u_i \cdot \nabla v_i - \int_\Gamma \frac{\partial u_i}{\partial n_i} v_i = \int_{\Omega_i} f_i v_i, \quad i = 1, 2. \tag{2.2}$$

Summing up the contributions of each subdomain and imposing the jump condition on the normal derivative (1.3) in a natural way, we obtain

$$\sum_{i=1}^{2} \int_{\Omega_i} \nabla u_i \cdot \nabla v_i - \int_\Gamma g_n v_i = \sum_{i=1}^{2} \int_{\Omega_i} f_i v_i \ . \tag{2.3}$$

Finally, using the decomposition (2.1), we obtain the weak form of problem (1.1)-(1.3): find $\bar{u} \in H^1_0(\Omega)$ such that $\forall v \in H^1_0(\Omega)$:

$$\int_\Omega \nabla \bar{u} \cdot \nabla v = \sum_{i=1}^{2} \int_{\Omega_i} f_i v_i - \sum_{i=1}^{2} \int_{\Omega_i} \nabla R_i g_d \cdot \nabla v_i + \int_\Gamma g_n v. \tag{2.4}$$

An alternative weak formulation of (1.1)-(1.3) was proposed by Huh and Sethian [12], by considering an additional lifting is considered for the function g_n. More precisely, they define a function $S_i g_n \in H^1_{\partial\Omega_i \setminus \Gamma}(\Omega_i), i = 1, 2$ such that $\left[\!\left[\frac{\partial S_i g_n}{\partial n} \right]\!\right]_\Gamma = g_n$ and, instead of (2.1), they consider the three-term splitting:

$$u_i = \hat{u}_i + R_i g_d + S_i g_n. \tag{2.5}$$

Remark that if for instance $g_n \in L^2(\Gamma)$, then the existence of $S_i g_n \in H^1_{\partial\Omega_i \setminus \Gamma}(\Omega_i)$ is ensured by the solution of the Neumann problem for the Laplace equation. The splitting (2.5) is similar to the one proposed in [4] in a finite difference context. The two liftings $R_i g_d$ and $S_i g_n$ should ideally satisfy the following constraints:

$$[\![R_i g_d]\!]_\Gamma = g_d \qquad \left[\!\!\left[\frac{\partial R_i g_d}{\partial n}\right]\!\!\right]_\Gamma = 0 \ , \tag{2.6}$$

$$[\![S_i g_n]\!]_\Gamma = 0 \qquad \left[\!\!\left[\frac{\partial S_i g_n}{\partial n}\right]\!\!\right]_\Gamma = g_n \ , \tag{2.7}$$

in which case they would take into account the jump of the functions and that of the fluxes independently.

Using these lifting operators, the following weak form of problem (1.1)-(1.3) can be derived: find $\hat{u} \in H^1_0(\Omega)$ such that, $\forall v \in H^1_0(\Omega)$,

$$\int_\Omega \nabla \hat{u} \cdot \nabla v = \sum_{i=1}^{2} \int_{\Omega_i} f_i v_i - \sum_{i=1}^{2} \int_{\Omega_i} \nabla (R_i g_d + S_i g_n) \cdot \nabla v_i + \int_\Gamma g_n v \ . \tag{2.8}$$

Note that $\hat{u}$ is such that $\hat{u}|_{\Omega_i} = \hat{u}_i$ for $i = 1, 2$.

We can remark that the bilinear form associated to both methods (2.4) and (2.8) is the classical Dirichlet formulation of the Poisson problem in $H^1_0(\Omega)$ (without internal discontinuity interface). This allows proving the well-posedness of the problem in a direct way by the Lax-Milgram lemma [20].

Both formulations (2.8) and (2.4) are equivalent from the mathematical point of view. Note that $\bar{u}$ and $\hat{u}$ have different regularity. In fact, the jump of normal derivatives of $\hat{u}$ is 0 across Γ whereas that of $\bar{u}$ isn't.
Obviously, their numerical approximation would yield different numerical solutions. We will discuss this issue in Sect. 5.1, while we focus now on the construction of the lifting operators R_i and S_i.

2.1. The continuous lifting operators. Formulations (2.4) and (2.8) require the knowledge of liftings of the jump conditions. If such liftings are already provided with the definition of the problem, they can be used without modifications and this section might be skipped. However, this is not the case that we will consider, as in general these liftings are not known.

In our approach to construct the liftings, we assume that there exist two continuous scalar functions $\bar{g}_d$ and $\bar{g}_n$ in Ω such that $g_d = \bar{g}_d|_\Gamma$ and $g_n = \bar{g}_n|_\Gamma$. We will discuss this point in Sect. 2.2.

Thanks to the extensions $\bar{g}_d$ and $\bar{g}_n$, we are able to define liftings that satisfy conditions (2.6) and (2.7) exactly at the continuous level. For the sake of simplicity, we start with the lifting for g_n which accounts for the jump in the normal derivative. From now on we assume to choose $\phi \in C^1(\bar{\Omega})$. Consider the function

$$S g_n = H(\phi) \phi \bar{g_n} \quad \text{in } \Omega, \tag{2.9}$$

where $H(\phi)$ is the Heaviside function of the domain $\Omega \setminus \Omega_1$:

$$H(\phi)(x) = \begin{cases} 1 & \text{if } \phi(x) \geq 0 \\ 0 & \text{if } \phi(x) < 0 \ , \end{cases}$$

whence

$$Sg_n(x) = \begin{cases} \phi(x)\bar{g_n}(x) & \text{if } \phi(x) \geq 0 \\ 0 & \text{if } \phi(x) < 0 \ . \end{cases} \tag{2.10}$$

Note that Sg_n is continuous across Γ (defined as the 0-level set of ϕ), that is $[\![Sg_n]\!]_\Gamma = 0$. On the other hand,

$$\left[\!\left[\frac{\partial Sg_n}{\partial n}\right]\!\right]_\Gamma = \frac{\partial(\phi\bar{g_n})}{\partial n}|_\Gamma = \frac{\partial\phi}{\partial n}|_\Gamma \ \bar{g_n}|_\Gamma + \frac{\partial\bar{g_n}}{\partial n}|_\Gamma \ \phi|_\Gamma = g_n \ , \tag{2.11}$$

thus Sg_n is a lifting of g_n which satisfies both conditions (2.7) are satisfied. We denote $(Sg_n)|_{\Omega_i}$ by $S_i g_n$. Notice that if $\bar{g}_n \in H^1(\Omega)$, then the variational problem (2.8) is well-posed for this choice of Sg_n.

Now we need a lifting Rg_d for the function g_d which is discontinuous across Γ but featuring a continuous normal derivative.
To this aim we define Rg_d as:

$$Rg_d = H(\phi)(\bar{g_d} - \phi\nabla\bar{g_d}\cdot\nabla\phi) \tag{2.12}$$

which can be expressed explicitly as

$$Rg_d(x) = \begin{cases} \bar{g_d}(x) - \phi(x)\nabla\bar{g_d}(x)\cdot\nabla\phi(x) & \text{if } \phi(x) \geq 0 \\ 0 & \text{if } \phi(x) < 0. \end{cases} \tag{2.13}$$

We can see that $[\![Rg_d]\!]_\Gamma = g_d$, whereas by a direct computation

$$\begin{aligned} \left[\!\left[\frac{\partial Rg_d}{\partial n}\right]\!\right]_\Gamma &= \frac{\partial(\bar{g_d} - \phi\nabla\bar{g_d}\cdot\nabla\phi)}{\partial n}|_\Gamma \\ &= \frac{\partial\bar{g_d}}{\partial n}|_\Gamma - \frac{\partial(\nabla\bar{g_d}\cdot\nabla\phi)}{\partial n}|_\Gamma \ \phi|_\Gamma - \frac{\partial\phi}{\partial n}|_\Gamma \ (\nabla\bar{g_d}\cdot\nabla\phi)|_\Gamma \\ &= \frac{\partial\bar{g_d}}{\partial n}|_\Gamma - \frac{\partial(\nabla\bar{g_d}\cdot\nabla\phi)}{\partial n}|_\Gamma \ 0 - 1 \ (\nabla\bar{g_d}\cdot n)|_\Gamma \\ &= \frac{\partial\bar{g_d}}{\partial n}|_\Gamma - \frac{\partial\bar{g_d}}{\partial n}|_\Gamma = 0. \end{aligned} \tag{2.14}$$

Therefore at the continuous level Rg_d is a lifting that satisfies conditions (2.6) (as before, we denote $R_i g_n = (Rg_n)|_{\Omega_i}$, $i = 1, 2$). If $\bar{g}_d \in H^2(\Omega)$, then we can guarantee that problem (2.8) is well-posed for the choice of Rg_d as in (2.12) since $R_i g_d \in H^1_{\partial\Omega_i\setminus\Gamma}(\Omega_i)$. Notice that by Sobolev embedding (see, e.g., [1]), $\bar{g}_d \in C^0(\bar{\Omega})$ for the one-, two- and three-dimensional cases.

REMARK 2.1. *Definitions* (2.9) *and* (2.12) *do not guarantee that the traces of Rg_d and Sg_n on $\partial\Omega$ are null. If this is not the case, one can construct suitable liftings (e.g., harmonic extensions) of the traces of Rg_d and Sg_n on $\partial\Omega$ and substract them from Rg_d and Sg_n to recover null traces. One should just pay attention to keep satisfying both conditions* (2.6) *and* (2.7)*, but this can be easily guaranteed by taking such liftings with support far enough from Γ.*

REMARK 2.2.

Finally, let us point out that to construct the liftings we could also use a more analytical approach instead of the ones illustrated before. A possibility would consist in solving a suitable PDE in each triangle crossed by the interface to play the role of

extension operators. To control both the trace and the normal derivative at the same time on the interface, we can solve a fourth order biharmonic problem in $K_i = K \cap \Omega_i$ for each K such that $K \cap \Gamma \neq \emptyset$. Precisely, the problem reads: find $R \in H^2(K_i)$ such that:

$$\Delta^2 R = 0 \quad \text{in } K_i \tag{2.15}$$

$$R = g_d \quad \text{on } K_\Gamma \tag{2.16}$$

$$\frac{\partial R}{\partial n} = g_n \quad \text{on } K_\Gamma. \tag{2.17}$$

Suitable Dirichlet and Neumann boundary conditions are then prescribed on $\partial_i K_i$ to close the problem and to keep the support of R restricted to Ω_Γ (K_Γ and $\partial_i K_i$ are defined as in figure 2.1).

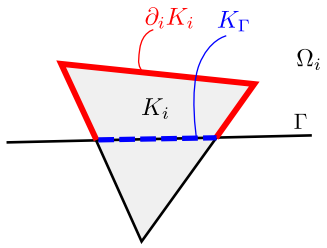

FIG. 2.1. *Illustration of the geometry of a triangle K cut by the interface Γ.*

EXAMPLE 2.1. *We consider a 1D example for the sake of clarity. The domain is $\Omega = (0,1)$ and the interface Γ is composed of the two points $x_1 = \pi^{-1}$ and $x_2 = 1 - \pi^{-1}$. The level set function is defined accordingly. We consider $\bar{g}_d(x) = \exp(2x)$ and $\bar{g}_n(x) = \sin(3x)$ so that $g_d(x_1) = \exp(2\pi^{-1})$, $g_d(x_2) = \exp(2(1-\pi^{-1}))$, $g_n(x_1) = \sin(3\pi^{-1})$ and $g_n(x_2) = \sin(3(1-\pi^{-1}))$. The explicit formula in this example are given by:*

$$Rg_d = \begin{cases} \exp(2x) + 2\exp(2x)(\pi^{-1} - x) & \text{if } x < \pi^{-1} \\ 0 & \text{if } \pi^{-1} < x < 1 - \pi^{-1} \\ \exp(2x) - 2\exp(2x)(x - 1 + \pi^{-1}) & \text{if } 1 - \pi^{-1} < x \end{cases}$$

$$Sg_n = \begin{cases} \sin(3x)(\pi^{-1} - x) & \text{if } x < \pi^{-1} \\ 0 & \text{if } \pi^{-1} < x < 1 - \pi^{-1} \\ \sin(3x)(x - 1 + \pi^{-1}) & \text{if } 1 - \pi^{-1} < x \end{cases}$$

The continuous liftings Rg_d and Sg_n are shown in figure 2.2.

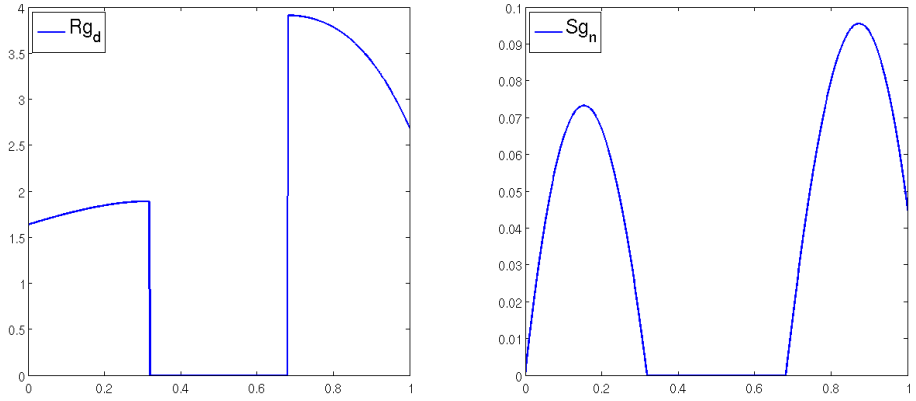

FIG. 2.2. *Continuous liftings obtained for the example 2.1: Rg_d (left) and Sg_n (right).*

EXAMPLE 2.2. *On the figure Fig.2.3, liftings for a 2D example (detailed in Sect. 5.2) are represented. In this example, the level set function is given by*

$$\phi(x,y) = \begin{cases} \sqrt{x^2+(y-0.5)^2} - 0.2 & \text{if } y > 0.5 \\ |x| - 0.2 & \text{if } |y| \leq 0.5 \\ \sqrt{x^2+(y+0.5)^2} - 0.2 & \text{if } y < -0.5 \end{cases}$$

and the exact solution (from which the jumps can be computed) by

$$u(x,y) = \begin{cases} 1 - \log(2\sqrt{x^2+y^2}) & \text{if } \phi(x,y) \geq 0 \\ 0 & \text{if } \phi(x,y) < 0 \ . \end{cases} \tag{2.18}$$

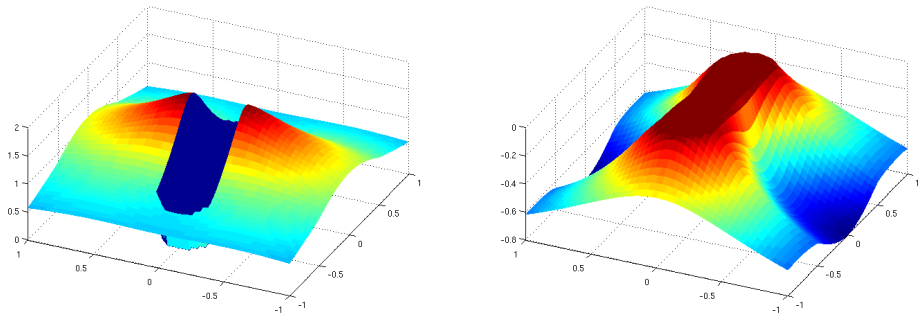

FIG. 2.3. *Continuous liftings Rg_d (left) and Sg_n (right) for a 2D problem.*

2.2. Extending interface data. In section 2.1, we supposed that extensions of the interface data g_d and g_n are already given and that they enjoy the required regularities. This assumption is more or less strong depending on the way the data g_d and g_n are provided. If they are given as functions on the whole domain Ω or as a

finite element function, this assumption is fulfilled. This is the case, for example, when one considers surface tension in a two phase flow problem: indeed, surface tension, which creates a jump in the pressure (see [14]), can be expressed in terms of the level set function and its derivative and therefore can naturally be defined on the whole domain of simulation. In other cases, this can be regarded as a strong limitation, then we provide here a method to overcome it. The method that we propose is based on the resolution of a PDE of Hamilton-Jacobi type. To extend the interface data g, we solve to steady state the following hyperbolic equation [19]:

$$\partial_t \bar{g} + S(\phi)\nabla\phi \cdot \nabla\bar{g} = 0 \tag{2.19}$$

where $S(\phi)$ represents the signature function, that is

$$S(\phi) = \begin{cases} 1 & \text{if } \phi > 0 \\ 0 & \text{if } \phi = 0 \\ -1 & \text{if } \phi < 0 \end{cases}$$

We remark that at steady state, $\bar{g}$ represents the extension of g by a function that is constant in the normal direction, i.e. $\nabla\phi \cdot \nabla\bar{g} = 0$. If this method is used to extend g_d from the interface, the formula (2.12) simplifies then to

$$Rg_d = H(\phi)\bar{g}_d \ . \tag{2.20}$$

For the sake of generality, in the rest of the paper we will consider the extension (2.12) so that the term $\nabla\phi \cdot \nabla\overline{g}_d$ will appear in our formulations. This term would not be present if instead one uses (2.20). Moreover, with this extension, the regularity required from $\bar{g}_d$ are lower than previously stated: we only need $\bar{g}_d \in H^1(\Omega)$ (instead of $H^2(\Omega)$) to ensure that the problem (2.8) is well-posed. The definition (2.9) remains unchanged for Sg_n.

REMARK 2.3. *In practice, the extension $\bar{g}_d$ and $\bar{g}_n$ are only required in those elements that are cut by the interface (see Sect. 3.1) and therefore, the equation* (2.19) *can be solved only in the region close to the interface.*

REMARK 2.4. *In 1D cases, this method leads to constant extensions in the vicinity of each interface point.*

3. Finite element approximation. In this section, we will address the numerical approximation of the problems introduced thus far, together with the introduction of the approximate lifting operators.

We consider a uniform triangulation τ_h of Ω made of elements K (intervals if $N = 1$, triangles if $N = 2$ or tetrahedra if $N = 3$). The interface Γ may intersect the elements K arbitrarily. As finite element space, we use the continuous $\mathbb{P}_1$ elements:

$$V_h = \{v_h \in H_0^1(\Omega) \cap C^0(\bar{\Omega}) \ : \ v_h|_K \in \mathbb{P}_1 \ \forall K \in \tau_h\}, \tag{3.1}$$

and we denote by $\{\Psi_j\}$ the basis functions of V_h.
The finite element approximation of (2.4) reads: find $\bar{u}_h \in V_h$ such that

$$\int_\Omega \nabla\bar{u}_h \cdot \nabla v_h = \int_\Gamma g_n v_h + \sum_{i=1}^{2} \int_{\Omega_i} f_i v_{hi} - \sum_{i=1}^{2} \int_{\Omega_i} \nabla R_i^h g_d \cdot \nabla v_{hi} \quad \forall v_h \in V_h, \tag{3.2}$$

while that of (2.8) becomes: find $\hat{u}_h \in V_h$ such that, for all $v_h \in V_h$,

$$\int_\Omega \nabla \hat{u}_h \cdot \nabla v_h = \int_\Gamma g_n v_h + \sum_{i=1}^{2} \int_{\Omega_i} f_i v_{hi} - \sum_{i=1}^{2} \int_{\Omega_i} \nabla (R_{hi} g_d + S_{hi} g_n) \cdot \nabla v_{hi} \ . \quad (3.3)$$

3.1. Discrete lifting operators. We introduce now suitable finite element approximations of the continuous liftings Rg_d and Sg_n. At the discrete level, we would like to have liftings with minimal support around the interface. Ideally, only the cells crossed by the interface would ought be used in order to keep the computational cost of the finite element approximation as low as possible. This is why the knowledge of the extensions $\bar{g}_d$ and $\bar{g}_n$ will be required only in those neighbooring cells.

Let $\pi_h^1 : C^0(\bar{\Omega}) \to V_h$ be the classical finite element interpolant operator

$$\pi_h^1(v) = \sum_j v(x_j)\Psi_j \quad (3.4)$$

that is $\pi_h^1(v)$ is the unique function in V_h which takes the same values of v at all finite element nodes x_j while Ψ_j is the characteristic basis function associated with x_j, that is $\Psi_j \in V_h : \Psi_j(x_i) = \delta_{ij}\ \forall i, j$ (see [22]).
Remark now that both liftings Rg_d and Sg_n that we have defined at the continuous level are the product of the Heaviside function by a continuous function. For all $t \in C^0(\bar{\Omega})$, define $T = H(\phi)t$ and then

$$\Pi_h^1(T)(x) = \begin{cases} \pi_h^1(t)(x) & \text{if } \phi(x) \geq 0 \\ 0 & \text{if } \phi(x) < 0. \end{cases} \quad (3.5)$$

Note that $\Pi_h^1(T) = \pi_h^1(t)H(\phi)$. We define then the discrete liftings $R_h^{glo} g_d = \Pi_h^1(Rg_d)$ and $S_h^{glo} g_n = \Pi_h^1(Sg_n)$. The index *glo* stands for *global* and it indicates that these functions are defined on the global domain Ω.

To guarantee that $Rg_d \in C^0(\bar{\Omega})$, we have to require a higher regularity for $\bar{g}_d$ than in Sect. 2.2. Indeed, if now $\bar{g}_d \in C^1(\bar{\Omega}) \cap H^2(\Omega)$, then $Rg_d \in C^0(\bar{\Omega}) \cap H^1(\Omega)$ so that $R_h^{glo} g_d$ is well defined and $R_i g_d,\ R_{ih} g_d \in H^1_{\partial\Omega_i \setminus \Gamma}(\Omega_i)$. Moreover, to ensure that $Sg_n \in C^0(\bar{\Omega})$, we now consider $\bar{g}_n \in C^0(\bar{\Omega}) \cap H^1(\Omega)$ so that $S_h^{glo} g_n$ is well-defined. Under these assumptions both formulations (2.8) and (3.3) are well-posed.

The regularity required on $\bar{g}_d$ is very strong. In case $\bar{g}_d$ does not satisfy it, one can resort to the procedure described in Sect. 2.2, which will lower the regularity requirement to $\bar{g}_d \in C^0(\bar{\Omega}) \cap H^1(\Omega)$. The above regularity assumptions might be further weakened if other types of interpolations (e.g., Clément interpolation [22] or Scott-Zhang interpolation [6]) were used instead of the Lagrangian one. Suitable projections (e.g. with respect to the L^2 or H^1 scalar product) might also be used in case of lower regularity.

EXAMPLE 3.1. *With the same settings of Example 2.1, we perform the interpolation on a mesh with* 5 *intervals using* $\mathbb{P}_1$ *finite elements. The resulting liftings are shown in figure 3.1.*

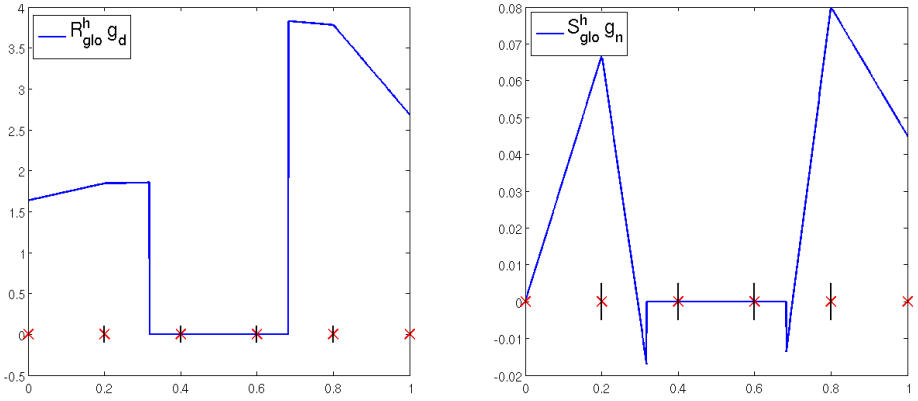

FIG. 3.1. *Discrete global liftings $R_h^{glo} g_d$ (left) and $S_h^{glo} g_n$ (right). The crosses show the location of the degrees of freedom.*

To reduce the computational cost induced by the fact that our liftings have global support, we introduce a region Ω_Γ of width h around the interface Γ (see Fig. 3.2) and we modify $R_h^{glo} g_d$ and $S_h^{glo} g_n$ so that the support of the modified functions be reduced to Ω_Γ. Notice that Ω_Γ corresponds to the strip of width h formed by those triangles that intersect the interface.

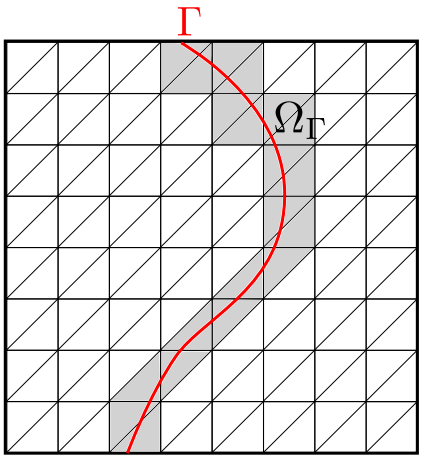

FIG. 3.2. *Illustration of Ω_Γ in a 2D case.*

We use the abstract notation T_h^{glo} to identify either $R_h^{glo} g_d$ or $S_h^{glo} g_n$. As by construction T_h^{glo} belongs to the discrete space V_h, we can express it on each side of the interface using the finite element basis:

$$T_h^{glo}|_K(x) = \begin{cases} \sum_i \alpha_i \Psi_i(x) & \text{if } \phi(x) \geq 0 \\ 0 & \text{if } \phi(x) < 0. \end{cases} \tag{3.6}$$

Adding any arbitrary function from the finite element space on both sides of the interface does not change the jump of this lifting. Then we can define a new lifting T_h as

$$T_h|_K = \begin{cases} T_h^{glo}|_K - \sum_{\phi_i \geq 0} \alpha_i \Psi_i & \text{if } K \cap \Gamma \neq \emptyset \\ -\sum_{\phi_i \geq 0} \alpha_i \Psi_i & \text{otherwise,} \end{cases} \tag{3.7}$$

where $\phi_i = \phi(x_i)$ and $\sum_{\phi_i \geq 0}$ is a simplified notation that stands for $\sum_{\{i:\phi_i \geq 0\}}$. Similar meaning for $\sum_{\phi_i < 0}$. By definition, the support of T_h is Ω_Γ. From the explicit expression of the lifting on the elements K crossed by the interface Γ:

$$T_h|_K(x) = \begin{cases} \sum_{\phi_i < 0} \alpha_i \Psi_i(x) & \text{if } \phi(x) \geq 0 \\ -\sum_{\phi_i \geq 0} \alpha_i \Psi_i(x) & \text{if } \phi(x) < 0, \end{cases} \tag{3.8}$$

we can see that T_h is actually 0 on $\partial\Omega_\Gamma$ and it is then extended by zero outside Ω_Γ. Applying this procedure to $R_h^{glo} g_d$ and $S_h^{glo} g_n$ we obtain the liftings $R_h g_d$ and $S_h g_n$ that fulfill all our requirements.

We can now give the explicit expression of the two liftings:

$$R_h g_d|_K(x) = \begin{cases} \sum_{\phi_i < 0} (\bar{g}_d(x_i) - \nabla \bar{g}_d(x_i) \cdot \nabla \phi(x_i)\ \phi(x_i)) \Psi_i(x) & \text{if } \phi(x) \geq 0 \\ -\sum_{\phi_i \geq 0} (\bar{g}_d(x_i) - \nabla \bar{g}_d(x_i) \cdot \nabla \phi(x_i)\ \phi(x_i)) \Psi_i(x) & \text{if } \phi(x) < 0, \end{cases} \tag{3.9}$$

$$S_h g_n|_K(x) = \begin{cases} \sum_{\phi_i < 0} (\bar{g}_n(x_i)\ \phi(x_i)) \Psi_i(x) & \text{if } \phi(x) \geq 0 \\ -\sum_{\phi_i \geq 0} (\bar{g}_n(x_i)\ \phi(x_i)) \Psi_i(x) & \text{if } \phi(x) < 0. \end{cases} \tag{3.10}$$

In case the interface coincides with the boundary of an element, the formulas (3.9) and (3.10) remain valid, in the sense that (2.6) and (2.7) are still approximated in a suitable way. In such a case, the correction will be taken into account only on those elements belonging to the subdomain characterized by negative values of the level set function.

EXAMPLE 3.2. *In figure 3.3 we show the new liftings $R_h g_g$ and $S_h g_n$ of reduced support corresponding to the functions of the example 2.1 using $\mathbb{P}_1$ polynomials.*

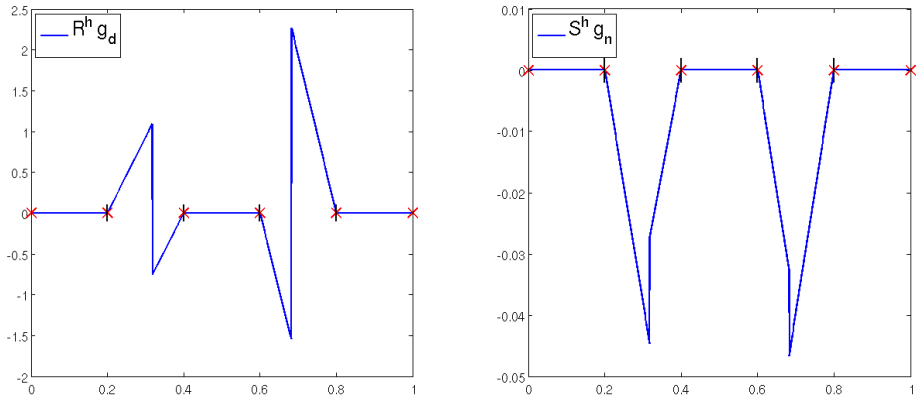

FIG. 3.3. *Liftings after the support reduction: $R_h g_d$ (left) and $S_h g_n$ (right). The crosses show the location of the degrees of freedom. These liftings should be compared to those in Fig. 3.1*

REMARK 3.1. *Remark that, thanks to the reduction of the support that we have performed, the extensions $\bar{g}_d$ and $\bar{g}_n$ of the interface data g_d and g_n have to be known only on Ω_Γ. This potentially reduces the cost of an extension procedure, e.g. the one described in Sect. 2.2.*

3.2. The SESIC method. The SESIC method that we propose is obtained by using the discrete lifting operators (3.9) and (3.10) in the context of the weak formulation (3.3). The only ingredient that remains to be detailed is the numerical integration formula that will be used to compute the new terms in the weak formulation (3.3). More precisely, we have to perform one integral on the interface Γ of a continuous function and two integrals over Ω of possibly discontinuous functions (indeed, both $\nabla R_h g_d$ and $\nabla S_h g_n$ might be discontinuous across Γ). We propose two different methods for the integration.

Two-side integration. The first method consists in building quadrature rules that take into account the interface. A possible way to integrate singular functions of type

$$\int_\Gamma f = \int_\Omega \delta_\Gamma f$$

is to reconstruct the interface Γ explicitly and then to use on it a $(N-1)$-dimensional quadrature rule. If $N = 1$, the interface reduces to a point and the integration requires only to evaluate f at a given point. If $N = 2$, the elements are triangles and then the interface in a single triangle is a segment in the case of a piecewise linear approximation. To apply a suitable integration rule on this segment, we need to compute the intersections of Γ with the edges of the triangle.

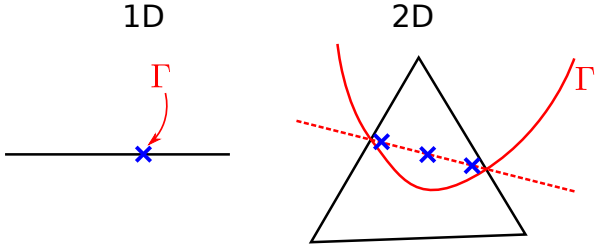

FIG. 3.4. *Illustration of the methods used for the computation of the line integral in 1D and 2D.*

On the other hand, to integrate discontinuous functions like

$$\int_\Omega f_1 + H(\phi) f_2,$$

we define a quadrature rule for an element crossed by Γ considering a quadrature rule on the polygons on each side of the interface. More precisely, if $N = 1$, we compute the location of the interface then we combine a quadrature rule for segments on each side of the interface. When $N = 2$, the triangles crossed by Γ are split into a triangle and a quadrilateral. To integrate discontinuous functions, we combine then a quadrature rule for triangles and a quadrature rule for quadrilaterals.

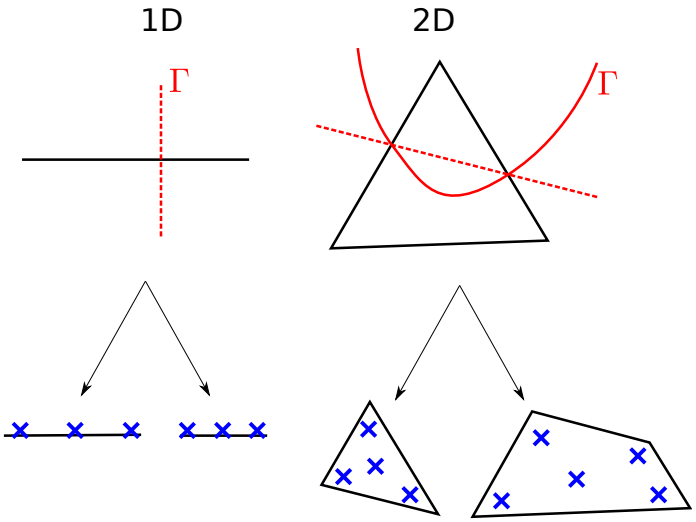

FIG. 3.5. *Illustration of the methods used for the computation of the discontinuous functions in 1D and 2D.*

Similar methods are available for 3D simulations, however they lead to complicated schemes where many different cases have to be distinguished depending on the way the interface cuts the tetrahedra. Thus we propose an alternative method that is simpler and more suitable for higher space dimensions or for higher polynomial degrees.

Integration of regularized functions. The idea, that can be adopted in any space dimension, is to approximate singular or discontinuous integrands by smooth functions. For example, we make the following approximation:

$$\int_\Gamma g_n v = \int_\Omega \bar{g}_n v \delta_\Gamma \cong \int_\Omega \bar{g}_n v \delta_w$$

where δ_w is an approximation of δ_Γ whose support is limited to a band of width w around Γ. This method is quite widely used, even if, often, there is no real control on the error produced. We refer to [25] for the error analysis of the regularization step, in which two errors are highlighted:

- the error (called "analytical error" in [25]) produced by the introduction of the regularizing function:
$$\left| \int_\Gamma g_n v - \int_\Omega \bar{g}_n v \delta_w \right| ;$$
- the quadrature error coming from the inexact integration of the regularized integrand.

The usual procedure is to take w as a given quantity of cells, meaning that w is proportional to h. However, the approach that we adopt in this paper is to use *a width w that is proportional to $\sqrt{h}$* (a similar width has been suggested in [14] in another context). Our choice is motivated by the following considerations. First of all, our function δ_w must have the form $\delta_w(d) = \frac{1}{w}\hat{\delta}(d/w)$ (prolongated by 0 outside the band of width w) where $\hat{\delta}$ is a function that does not depend on w, the factor $\frac{1}{w}$ making the weight of δ_w constant with respect to w, and d is the distance to the interface, that is $d(x) = \phi(x)$.

- The error analytical is then proportional to w^β, where β can be computed using the properties (vanishing moments) of $\hat{\delta}$ [25].
- If the integrand $\bar{g}_n v \delta_w$ is a function of $C^m(\Omega)$ and the quadrature rule (based on the finite element mesh, with typical size h) has a degree of exactness $m-1$ (see [21]), the quadrature error is proportional to $h^m ||(g_n v \delta_w)^{(m)}||_{L^\infty(\Omega)}$. However, $\delta_w^{(m)}$ scales like $w^{-(m+1)}$. Therefore, the quadrature error is dominated by $h^m w^{-(m+1)}$.

Based on these arguments, we derive that, by choosing $w = h$ we cannot ensure that the quadrature error will vanish when $h \to 0$. Indeed, with $w = h$, the number of quadrature points in the band of width w is constant while the function δ_w is becoming steeper to conserve the mass. Our choice of $w = c\sqrt{h}$ leads to control the analytical error by $h^{\beta/2}$ and the quadrature error by $h^{(m-1)/2}$. We can then fully control the decay rate of the overall error by choosing the appropriate $\hat{\delta}$ function.

If we look for second order accuracy, building $\hat{\delta}$ with 3 vanishing moments (then $\beta = 4$, see [25]) and 5 continuous derivatives would be sufficient. By looking for the polynomial function with the smallest degree featuring these properties, we end up with:

$$\hat{\delta}(d) = \frac{6435}{8192}(3 - 35d^2 + 147d^4 - 315d^6 + 385d^8 - 273d^{10} + 105d^{12} - 17d^{14}) \quad (3.11)$$

A representation of this function is given in Fig. 3.6.

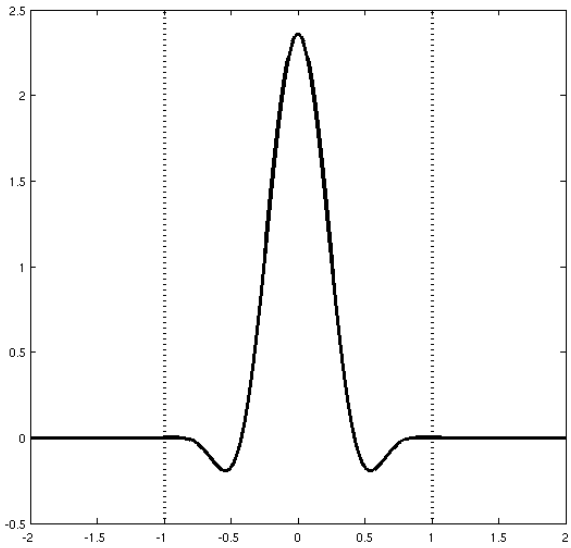

FIG. 3.6. *Plot of the function* $\hat{\delta}(d)$

The same approach can be applied for the Heaviside function to integrate discontinuous integrand across the interface. We used for our tests the regularized Heaviside function:

$$\hat{H}(d) = \int_{-1}^{d} \hat{\delta}(\xi)\ d\xi.$$

To illustrate our choice for the integration, we consider 3 examples in 2D, where the domain is the square $\Omega = (-1, 1)^2$ and the triangulation is made by triangles whose typical size is denoted by h. All the integrations are performed using a Dunavant quadrature rule of degree 4 in all the triangles of the mesh [9]. For each example, we will use three different methods to evaluate a line integral on the 0 level set of the function ϕ:

- **Method A:** The bandwith is set to $w = 2h$ and we take $\hat{\delta}(d) = (1 + \cos(\pi d))/2$.
- **Method B:** The bandwith is set to $w = 2h$ and $\hat{\delta}$ is defined as in (3.11).
- **Method C:** The bandwith is set to $w = \sqrt{h}/2$ and $\hat{\delta}$ is again as in (3.11).

EXAMPLE 3.3. *The first example consists in simply calculating the length of a circle. The level set function is defined as* $\phi(x, y) = \sqrt{x^2 + y^2} - 0.5$. *In this example, the error is due only to the quadrature error. Figure 3.7 shows the magnitude of the error as function of the mesh size* h. *We can remark that with methods A and B the convergence quickly slows down to order of at most* 1, *while method C yields a convergence rate of order* 4.

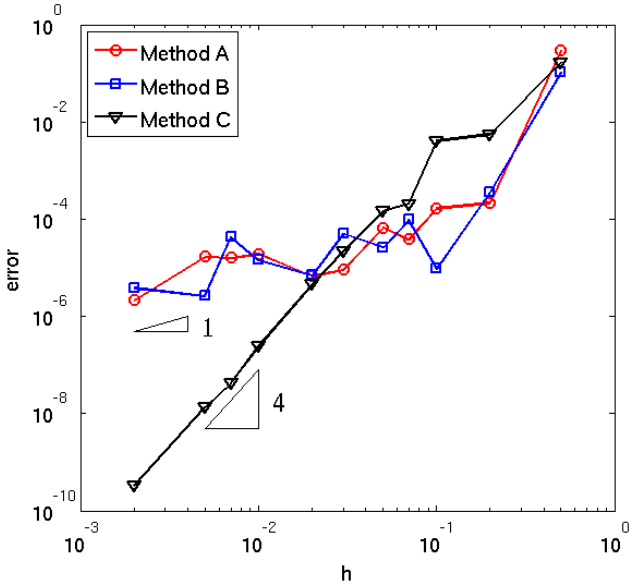

FIG. 3.7. *Results of example 3.3.*

EXAMPLE 3.4. *The second example consists in integrating on a quarter of circle the function* $f(x, y) = (y + 1)\exp(x + 1)$. *The level set function is* $\phi(x, y) = \sqrt{(x + 1)^2 + (y + 1)^2} - 1.5$. *Figure 3.8 shows the results obtained. We can see that the methods A and B give rise to a good convergence for coarse meshes, but the convergence slows down at a level comparable to the one observed in example 3.3. Method C is more robust as it yields again a convergence rate close to* 2 *for the whole range of meshes tested.*

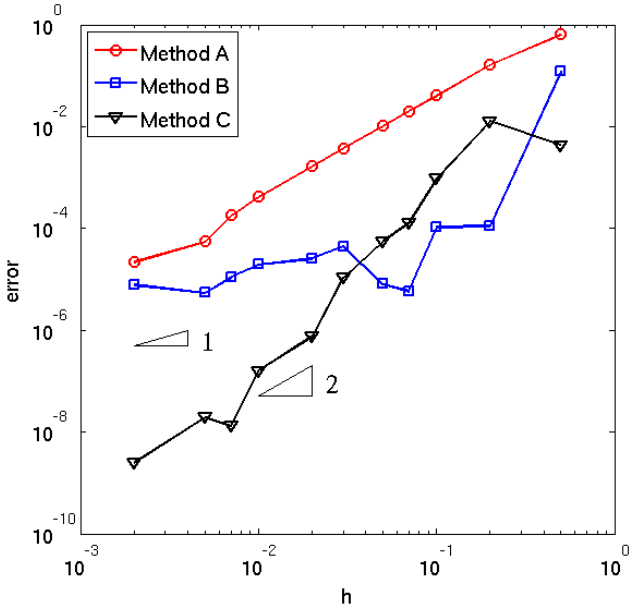

FIG. 3.8. *Results of example 3.4.*

EXAMPLE 3.5.

The last example consists again in computing the length of a curve. However, the curve that we consider has just a C^0 regularity (see Fig. 3.9 left). As shown in Fig. 3.9 (right), the convergence rates for the methods A, B and C are lower than in the previous examples. We can also remark that method C yields a slower convergence in this example.

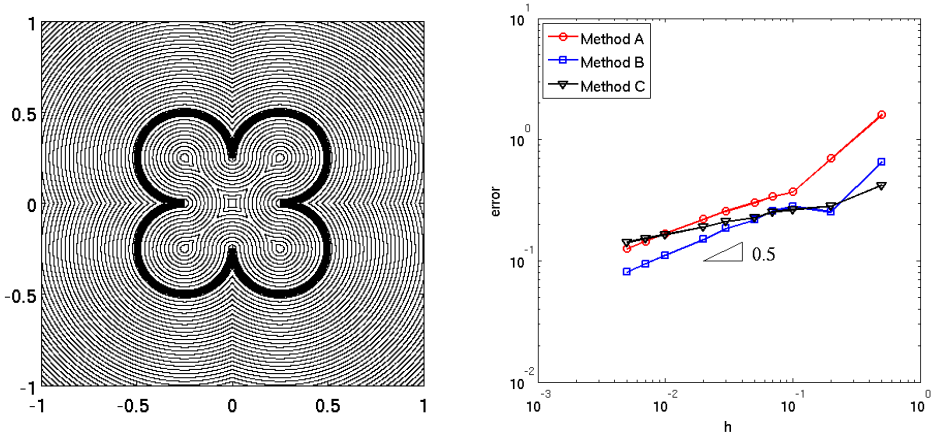

FIG. 3.9. *Representation of the isocurves of the level set function (left, Γ in bold) and magnitude of the error on the comptation of the length of the curve.*

From these examples, we can see that in case the level set function has a lower regularity than $C^1(\bar{\Omega})$, as we assumed in this paper, method C might underperform

with respect to methods A and B. Indeed, when the regularity is low, the integration error might be controlled by a term of the form w^α where $\alpha > 0$ is relatively small (around 0.5 in example 3.5). In such a case, choosing w proportional to $\sqrt{h}$ might give worse results than if it is proportional to h. Similar remarks hold for 3D cases.

3.3. On the choice of the discrete lifting operator. In the previous section 3.1, we proposed a particular construction of the lifting operators that is interesting as it does not require to reconstruct the interface. We shall demonstrate here that the solution u_h obtained using the SESIC method is actually independent of this construction to a certain extent.

Suppose that we consider a suitable discrete lifting $\tilde{T}_h = \tilde{T}_h(g_d, g_n)$ such that $R_h g_d + S_h g_n - \tilde{T}_h \in V_h$. As a consequence

- $\tilde{T}_h$ is linear is each subdomain Ω_i, $i = 1, 2$;
- the interface conditions are satisfied in the same way as with our construction in the sense that they satisfy the same jumps across the interface at the discrete level.

Using the discrete formulation of the SESIC method (3.3), we denote by $\hat{w}_h \in V_h$ the solution obtained considering the lifting $\tilde{T}_h$, i.e., for all $v_h \in V_h$,

$$\int_\Omega \nabla \hat{w}_h \cdot \nabla v_h = \int_\Gamma g_n v_h + \sum_{i=1}^{2} \int_{\Omega_i} f_i v_{hi} - \sum_{i=1}^{2} \int_{\Omega_i} \nabla \tilde{T}_h \cdot \nabla v_{hi} \ . \tag{3.12}$$

We now prove that $w_h = \hat{w}_h + \tilde{T}_h$ coincides with u_h. Substracting (3.12) from (3.3), we obtain, for all $v_h \in V_h$,

$$\int_\Omega \nabla(u_h - w_h) \cdot \nabla v_h = 0 \ . \tag{3.13}$$

We have $u_h - w_h = (\hat{u}_h + Rg_d + Sg_n) - (\hat{w}_h + \tilde{T}_h) \in V_h$ as by definition $\hat{u}_h \in V_h$, $\hat{w}_h \in V_h$ and $R_h g_d + S_h g_n - \tilde{T}_h \in V_h$ by assumption. Since the Galerkin approximation of the Laplace problem is well-posed on V_h, from (3.13) it follows that $u_h - w_h = 0$.

In view of this result, we can now comment on the case of 1D problems. As already remarked, using the extension of the interface data proposed in Sect. 2.2, $\bar{g}_d$ and $\bar{g}_n$ are constant in the vicinity of the interface (that might be composed of several points). Thanks to the definitions (2.9) and (2.20) and to the fact that the level set function ϕ is piecewise linear in 1D, Rg_d and Sg_n are piecewise linear in the neighborhood of the interface. Therefore, the interpolation step (3.5) leaves Rg_d and Sg_n unchanged and the jump conditions (2.6) and (2.7) are satisfied exactly. This implies that in 1D, any construction of the liftings using piecewise linear functions and satisfying exactly the interface conditions yields the same solution as the SESIC method.

Based on this argument we can conclude, that in the 1D case, the SESIC method is a special XFEM method based on the formulation in [13] with the two following differences:

1. in SESIC both interfaces conditions are imposed strongly, whilst in [13] only the condition (1.2) is imposed strongly;
2. in SESIC the enriched basis functions are piecewise linear whereas they are piecewise quadratic in [13].

The above analogies do not hold for multidimensional problem.

3.4. The ESIC method. As stated before, the SESIC was inspired by the ESIC method first proposed in [12]. For the sake of comparison, let us recall the principle of the ESIC method and emphasize the differences with the new SESIC method.

The two methods are built on different weak formulations of the given problem (1.1)-(1.3). SESIC stems from the weak form (3.3) whereas in order to get rid of the line integral in (3.3), Huh and Sethian perform a counter integration by parts yielding:

$$\int_\Gamma g_n v_h - \sum_{i=1}^{2} \int_{\Omega_i} \nabla S_i g_n \cdot \nabla v_{hi} = \sum_{i=1}^{2} \sum_K \int_{K\cap\Omega_i} \Delta S_i g_n v_{hi} - \sum_{i=1}^{2} \sum_K \int_{\partial K} \frac{\partial S_i g_n}{\partial n} v_{hi}\,. \quad (3.14)$$

However, this formulation introduces a new error source, as it makes use of the equality $g_n = \left[\!\left[\frac{\partial S g_n}{\partial n}\right]\!\right]$, which might be wrong at the discrete level. This is in fact documented by the numerical tests that we will present in section 5.

The second major difference relies on the construction of the lifting operators. According to [12], the extension $\tilde{g_*}$ on Ω_Γ of a generic function g_* defined only on Γ is defined as follows

$$\tilde{g_*}(x) = g_*(x_\Gamma) \quad \text{for all } x \in \Omega_\Gamma, \quad (3.15)$$

where x_Γ is the point of Γ that minimizes the distance to x. As a consequence, $\tilde{g_*}$ is constant along any normal direction issuing from Γ.

Let now $\tilde{g_d}$ be the extension in Ω_Γ of g_d according to (3.15). Then, considering the triangulation of Ω and the basis $\{\Psi_j\}$ of V_h (3.1), in [12] the lifting is defined as follows

$$\tilde{R} g_d = \begin{cases} -\sum_{\phi_j \geq 0} \Psi_j \tilde{g_d} & \text{in } \Omega_1 \\ \sum_{\phi_j < 0} \Psi_j \tilde{g_d} & \text{in } \Omega_2. \end{cases} \quad (3.16)$$

By construction, $\tilde{R} g_d$ has the prescribed jump $[\![\tilde{R} g_d]\!]_\Gamma = g_d$ and it has continuous normal derivative across Γ: $\left[\!\left[\frac{\partial \tilde{R} g_d}{\partial n}\right]\!\right]_\Gamma = 0$. At the discrete level, the lifting becomes:

$$\tilde{R}_h g_d = \begin{cases} -\sum_{\phi_j \geq 0} \Psi_j \tilde{g_d}_j & \text{in } \Omega_1 \\ \sum_{\phi_j < 0} \Psi_j \tilde{g_d}_j & \text{in } \Omega_2, \end{cases} \quad (3.17)$$

where $\tilde{g_d}_j$ denotes the value of the function $\tilde{g_d}$ at the node x_j. In this case, the jumps through the interface are satisfied in an interpolation sense: indeed it is $[\![\tilde{R}_h g_d]\!]_\Gamma = \sum_j \tilde{g_d}_j \Psi_j$ and $\left[\!\left[\frac{\partial \tilde{R}_h g_d}{\partial n}\right]\!\right]_\Gamma = \sum_j \tilde{g_d}_j \frac{\partial \Psi_j}{\partial n}$.

The potential disadvantage of this methodology with respect to the approach that we have developed in the previous section 3.1 is that the interface has to be reconstructed since in (3.15) the closest point x_Γ is requested and, according to [12], this operation has to be performed using the interface explicitly.

A similar approach is proposed in [12] to construct the lifting of g_n. Note that after multiplying a function built as in (3.17) by the level-set function ϕ, it becomes

continuous across the interface (since ϕ is equal to 0 on the interface), while its normal derivative exhibits a jump of the desired magnitude. So, after constructing $\tilde{g_n}$ as in (3.15), the discrete lifting for g_n becomes:

$$\tilde{S}_h g_n = \begin{cases} -\sum_{\phi_j \geq 0} \Psi_j \tilde{g_n}_j \phi & \text{in } \Omega_1 \\ \sum_{\phi_j < 0} \Psi_j \tilde{g_n}_j \phi & \text{in } \Omega_2. \end{cases} \tag{3.18}$$

The potential drawback of this construction is that the multiplication by ϕ increases the polynomial order of the lifting function, thus requiring a polynomial refinement in the neighborhood of the interface. Moreover, the closest point extension requires again to rebuild the interface explicitly.

REMARK 3.2. *The construction of the liftings of Sect. 3.1 can be seen as a generalization of those presented in this section and used in the ESIC method. Indeed, if instead of the extensions of g_* introduced in Sect. 2.1, we took the closest point extension (3.15), then the liftings $R_h g_d$ and $S_h g_n$ would coincide with (3.17) and (3.18). Notice again that in Sect. 3.1 we do not need at all to reconstruct Γ.*

3.5. Higher order approximations. Our construction concerns only linear finite elements. However, it can be generalized to higher order polynomial approximation. Indeed, only the finite element space (3.1) and the interpolation operator (3.5) have to be adapted.

The reason for treating only the linear case resides in the regularity of $\hat{u}$. Indeed, thanks to the construction of the liftings, we know that $\hat{u} \in H^2(\Omega)$, but it is not possible to ensure more regularity, e.g. $H^3(\Omega)$, as the liftings introduced so far do not provide control on second order derivatives across the interface. The use of higher order polynomial for the approximation would not be necessarily rewarded by an higher convergence rate, in particular close to the interface.

In order to achieve higher convergence rate, one would need to build liftings that correct the second (and possibly higher) derivatives. This can be done by considering functions of the type [private communication with Huh and Sethian]

$$L_k g = H(\phi)\phi^k g \tag{3.19}$$

which have $k-1$ continuous derivatives across Γ and yield a jump in the k^{th} derivative. The solution would then be further decomposed, following (2.1) and (2.5):

$$u_i = \bar{u}_i + R_i g_d + S_i g_n + \sum_{j=2}^{l} L_i^j g \tag{3.20}$$

and the weak formulation would be changed accordingly.

4. Error analysis. For the sake of analysis, besides the regularity assumptions made in the previous sections, we also suppose that the restrictions of the continuous liftings Rg_d and Sg_n to Ω_i belong to $H^2(\Omega_i)$, $i = 1, 2$. Throughout this section we will denote by C a suitable constant which may change in the different inequalities, but that will always be independent of h.

In this section, we carry out the error analysis of the SESIC method, using the weak formulation (3.3). To perform the analysis, we will use exclusively the liftings $R_h^{glo} g_d$

and $S_h^{glo} g_n$, as they have continuous counterparts to which they can be compared. However, in practice, one would rather use the liftings $R_h g_d$ and $S_h g_n$. The following argument shows that our analysis also stands for this latter couple of liftings.

Let us denote by $\hat{u}_h$ the solution of the problem (3.3) using $R_h g_d$ and $S_h g_n$, $u_h = \hat{u}_h + R_h g_d + S_h g_n$, $\hat{u}_h^{glo}$ the solution of problem (3.3) using $R_h^{glo} g_d$ and $S_h^{glo} g_n$ and $u_h^{glo} = \hat{u}_h^{glo} + R_h^{glo} g_d + S_h^{glo} g_n$. First of all, we remark that $u_h - u_h^{glo} \in V_h$, as $\hat{u}_h, \hat{u}_h^{glo} \in V_h$ by definition and $R_h g_d - R_h^{glo} g_d \in V_h$, $S_h g_n - S_h^{glo} g_n \in V_h$ because of the way the support reduction has been performed in Sect. 3.1. Because both $\hat{u}_h$ and $\hat{u}_h^{glo}$ satisfy (3.3), we have:

$$\int_\Omega \nabla(u_h - u_h^{glo}) \cdot \nabla v_h = 0 \qquad \forall v_h \in V_h \ . \tag{4.1}$$

Since the Galerkin approximation of the Laplace problem is well-posed on V_h, $u_h - u_h^{glo}$ is the unique solution. As 0 is also a solution of that problem, these two solutions must coincide: $u_h - u_h^{glo} = 0$. Therefore, the two lifting sets yield the same final solution and so the convergence analysis carried out for u_h^{glo} also applies to u_h.

In order to obtain *a-priori* error estimates, we split the error into three parts:

$$u - u_h^{glo} = (\hat{u} + Rg_d + Sg_n) - (\hat{u}_h^{glo} + R_h^{glo} g_d + S_h^{glo} g_n) \tag{4.2}$$

whence

$$||u - u_h^{glo}|| \leq ||\hat{u} - \hat{u}_h^{glo}|| + ||Rg_d - R_h^{glo} g_d|| + ||Sg_n - S_h^{glo} g_n|| \tag{4.3}$$

where $||\cdot||$ represents a suitable norm. Using the construction of the lifting operators and the classical interpolation error estimates for the operator π_h^1 (see, e.g., [22]), the last two terms may be bounded as follows:

$$\sum_{i=1}^{2} ||T - T_h^{glo}||_{H^1(\Omega_i)} \leq Ch \sum_{i=1}^{2} |T|_{H^2(\Omega_i)} \ , \tag{4.4}$$

$$\sum_{i=1}^{2} ||T - T_h^{glo}||_{L^2(\Omega_i)} \leq Ch^2 \sum_{i=1}^{2} |T|_{H^2(\Omega_i)} \ , \tag{4.5}$$

where T (respectively, T_h^{glo}) denotes either Rg_d or Sg_n (respectively, $R_h^{glo} g_d$ or $S_h^{glo} g_n$).

Thus, we need to estimate the first term in (4.3). The analysis that we will carry out in this section does not rely on a specific construction of the lifting operators and could be applied directly to other constructions.

4.1. Convergence in the H^1 norm. To quantify the convergence in the energy norm, we use the first Strang lemma [22] (in our case, the bilinear forms of the continuous and discrete weak formulations coincide):

$$\begin{aligned}||\hat{u} - \hat{u}_h^{glo}||_{H^1(\Omega)} \leq \left(1 + \frac{\gamma}{\alpha}\right) \inf_{w_h \in V_h} ||\hat{u} - w_h||_{H^1(\Omega)} \\ + \frac{1}{\alpha} \sup_{v_h \in V_h} \frac{1}{||v_h||_{H^1(\Omega)}} \left| \sum_{i=1}^{2} \int_{\Omega_i} \nabla(Rg_d + Sg_n) \cdot \nabla v_h \right. \\ \left. - \sum_{i=1}^{2} \int_{\Omega_i} \nabla(R_h^{glo} g_d + S_h^{glo} g_n) \cdot \nabla v_h \right|\end{aligned} \tag{4.6}$$

where γ is the continuity constant of the bilinear form $a(u,v) = \int_\Omega \nabla u \cdot \nabla v$ and α its coercivity constant. The first term on the right hand side can be bounded thanks to the properties of the finite element space used, i.e., linear Lagrangian functions:

$$\inf_{w_h \in V_h} ||\hat{u} - w_h||_{H^1(\Omega)} \leq Ch|\hat{u}|_{H^2(\Omega)} \ . \tag{4.7}$$

For the second term, using the Cauchy-Schwarz inequality, we obtain:

$$\begin{aligned}&|\sum_{i=1}^{2} \int_{\Omega_i} \nabla(Rg_d + Sg_n) \cdot \nabla v_h - \int_{\Omega_i} \nabla(R_h^{glo} g_d + S_h^{glo} g_n) \cdot \nabla v_h| \\ &= |\sum_{i=1}^{2} \int_{\Omega_i} \nabla(Rg_d - R_{glo}^h g_d + Sg_n - S_{glo}^h g_n) \cdot \nabla v_h| \\ &\leq \left(\sum_{i=1}^{2} |(Rg_d - R_{glo}^h g_d) + (Sg_n - S_{glo}^h g_n)|_{H^1(\Omega_i)} \right) ||v_h||_{H^1(\Omega)} \ .\end{aligned}$$

Therefore, thanks to the triangular inequality and the error estimate (4.4), we have

$$\sup_{v_h \in V_h} \frac{1}{||v_h||_{H^1(\Omega)}} \left| \sum_{i=1}^{2} \int_{\Omega_i} \nabla(Rg_d + Sg_n) \cdot \nabla v_h \right. \tag{4.8}$$

$$\left. - \sum_{i=1}^{2} \int_{\Omega_i} \nabla(R_h^{glo} g_d + S_h^{glo} g_n) \cdot \nabla v_h \right| \tag{4.9}$$

$$\leq \sum_{i=1}^{2} \left(|(Rg_d - R_h^{glo} g_d) + (Sg_n - S_h^{glo} g_n)|_{H^1(\Omega_i)} \right) \tag{4.10}$$

$$\leq Ch \sum_{i=1}^{2} (|Rg_d|_{H^2(\Omega_i)} + |Sg_n|_{H^2(\Omega_i)}) \ . \tag{4.11}$$

To sum up, we have:

$$||\hat{u} - \hat{u}_h^{glo}||_{H^1(\Omega)} = Ch|\hat{u}|_{H^2(\Omega)} + Ch \sum_{i=1}^{2} (|Rg_d|_{H^2(\Omega_i)} + |Sg_n|_{H^2(\Omega_i)}) \tag{4.12}$$

so that $\hat{u}_h^{glo}$ converges towards $\hat{u}$ with order 1 in H^1 norm, and thanks to (4.3), we have also optimal convergence of u_h^{glo} towards u:

$$\sum_{i=1}^{2} ||u - u_h^{glo}||_{H^1(\Omega_i)} \leq Ch(|\hat{u}|_{H^2(\Omega)} + \sum_{i=1}^{2} |Rg_d|_{H^2(\Omega_i)} + \sum_{i=1}^{2} |Sg_n|_{H^2(\Omega_i)}). \quad (4.13)$$

4.2. Convergence in the L^2 norm. We define $e_h = u - u_h^{glo} \in L^2(\Omega)$ the total error done by our scheme, and $\hat{e}_h = \hat{u} - \hat{u}_h^{glo} \in H_0^1(\Omega)$. Then, for a fixed $h > 0$, we define $\psi \in H_0^1(\Omega)$ the solution of the following dual problem:

$$\int_\Omega \nabla v \cdot \nabla \psi = \int_\Omega \hat{e}_h v \qquad \forall v \in H_0^1(\Omega) \ . \quad (4.14)$$

Using $v = \hat{e}_h$ in the previous relation, we have

$$||\hat{e}_h||^2_{L^2(\Omega)} = \int_\Omega \nabla \hat{e}_h \cdot \nabla \psi \quad (4.15)$$

which is equivalent to

$$||\hat{e}_h||^2_{L^2(\Omega)} = \sum_{i=1}^{2} \int_{\Omega_i} \nabla e_h \cdot \nabla \psi + \sum_{i=1}^{2} \int_{\Omega_i} \nabla(\hat{e}_h - e_h) \cdot \nabla \psi \quad (4.16)$$

We shall now analyse the two terms on the right hand side separately. For the first term we follow the usual *Aubin-Nitsche argument*. Using Galerkin's othogonality, we have for any $w_h \in V_h$:

$$\begin{aligned} \sum_{i=1}^{2} \int_{\Omega_i} \nabla e_h \cdot \nabla \psi &= \sum_{i=1}^{2} \int_{\Omega_i} \nabla e_h \cdot \nabla(\psi - w_h) \\ &\leq \sum_{i=1}^{2} ||e_h||_{H^1(\Omega_i)} ||\psi - w_h||_{H^1(\Omega_i)} \\ &\leq 2||\psi - w_h||_{H^1(\Omega)} \sum_{i=1}^{2} ||e_h||_{H^1(\Omega_i)} \ . \end{aligned} \quad (4.17)$$

Therefore,

$$\begin{aligned} \sum_{i=1}^{2} \int_{\Omega_i} \nabla e_h \cdot \nabla \psi &\leq 2 \inf_{w_h \in V_h} ||\psi - w_h||_{H^1(\Omega)} \sum_{i=1}^{2} ||e_h||_{H^1(\Omega_i)} \\ &\leq Ch||\psi||_{H^2(\Omega)} \sum_{i=1}^{2} ||e_h||_{H^1(\Omega_i)} \ . \end{aligned} \quad (4.18)$$

Regarding the second term in (4.16), we have, as the liftings are defined to be 0 in Ω_1,

$$\sum_{i=1}^{2}\int_{\Omega_i}\nabla(\hat{e}_h-e_h)\cdot\nabla\psi=\int_{\Omega_2}\nabla(Sg_n+Rg_d-S_h^{glo}g_n-R_h^{glo}g_d)\cdot\nabla\psi\ . \tag{4.19}$$

By a counter integration by parts, we obtain:

$$\begin{aligned}
&\sum_{i=1}^{2}\int_{\Omega_i}\nabla(\hat{e}_h-e_h)\cdot\nabla\psi\\
&=-\int_{\Omega_2}(Sg_n+Rg_d-S_h^{glo}g_n-R_h^{glo}g_d)\ \Delta\psi\\
&\quad+\int_{\partial\Omega_2}\frac{\partial\psi}{\partial n}(Sg_n+Rg_d-S_h^{glo}g_n-R_h^{glo}g_d)\\
&=-\int_{\Omega_2}(Sg_n+Rg_d-S_h^{glo}g_n-R_h^{glo}g_d)\ \Delta\psi\\
&\quad+\int_{\Gamma}\frac{\partial\psi}{\partial n}(Sg_n+Rg_d-S_h^{glo}g_n-R_h^{glo}g_d)
\end{aligned} \tag{4.20}$$

as the liftings have null trace on $\partial\Omega$. Using Cauchy-Schwarz inequality and a trace inequality, we have:

$$\begin{aligned}
&\sum_{i=1}^{2}\int_{\Omega_i}\nabla(\hat{e}_h-e_h)\cdot\nabla\psi\\
&\leq||Sg_n+Rg_d-S_h^{glo}g_n-R_h^{glo}g_d||_{L^2(\Omega_2)}||\Delta\psi||_{L^2(\Omega_2)}\\
&\quad+||Sg_n+Rg_d-S_h^{glo}g_n-R_h^{glo}g_d||_{L^2(\Gamma)}||\frac{\partial\psi}{\partial n}||_{L^2(\Omega)}\\
&\leq C\Big(||Sg_n+Rg_d-S_h^{glo}g_n-R_h^{glo}g_d||_{L^2(\Omega)}\\
&\quad+||Sg_n+Rg_d-S_h^{glo}g_n-R_h^{glo}g_d||_{L^2(\Gamma)}\Big)\ ||\psi||_{H^2(\Omega)}\ .
\end{aligned} \tag{4.21}$$

All together, (4.16) gives

$$\begin{aligned}
||\hat{e}_h||^2_{L^2(\Omega)}\leq&\Big(Ch\sum_{i=1}^{2}||e_h||_{H^1(\Omega_i)}+||Sg_n+Rg_d-S_h^{glo}g_n-R_h^{glo}g_d||_{L^2(\Omega)}\\
&+||Sg_n+Rg_d-S_h^{glo}g_n-R_h^{glo}g_d||_{L^2(\Gamma)}\Big)||\psi||_{H^2(\Omega)}
\end{aligned} \tag{4.22}$$

Thanks to the elliptic regularity, we have $||\psi||_{H^2(\Omega)}\leq C||\hat{e}_h||_{L^2(\Omega)}$, so

$$\begin{aligned}
||\hat{e}_h||_{L^2(\Omega)}\leq Ch||e_h||_{H^1(\Omega)}+||Sg_n+Rg_d-S_h^{glo}g_n-R_h^{glo}g_d||_{L^2(\Omega)}\\
+||Sg_n+Rg_d-S_h^{glo}g_n-R_h^{glo}g_d||_{L^2(\Gamma)}
\end{aligned} \tag{4.23}$$

Using the H^1 error estimate that we have already derived and the interpolation errors for the liftings (4.5) and [23], we have:

$$||\hat{e}_h||_{L^2(\Omega)} \leq Ch^2 \left(|\hat{u}|_{H^2(\Omega)} + \sum_{i=1}^{2} |Rg_d|_{H^2(\Omega_i)} + \sum_{i=1}^{2} |Sg_n|_{H^2(\Omega_i)} + |Rg_d|_{H^2(\Gamma)} + |Sg_n|_{H^2(\Gamma)} \right), \tag{4.24}$$

where we have supposed that Rg_d and Sg_n are regular enough so that the norms on the right hand side are well defined.

5. Numerical results. In this section, we present numerical results obtained using the methodologies described in the previous sections for different geometric dimensions.

5.1. 1D test case. First of all, we consider a 1D Poisson problem, as this allows us to make complete error measurements and visualizations. We consider the unit interval $\Omega = (0, 1)$ with an interface located in $\Gamma = \{\pi^{-1}\}$ so that the uniform meshes that we will use will not conform with the interface. The level set function is defined as $\phi(x) = \pi^{-1} - x$. The Poisson problem consists in finding $u : \Omega \to \mathbb{R}$ such that

$$\begin{aligned} -u''(x) &= -e^x \quad \text{in } \Omega \\ u(0) &= 1 \\ u(1) &= e + 2, \end{aligned} \tag{5.1}$$

with the jump conditions

$$[\![u]\!]_\Gamma = -2\pi^{-1} \qquad \left[\!\!\left[\frac{\partial u}{\partial n}\right]\!\!\right]_\Gamma = 2. \tag{5.2}$$

The exact solution reads

$$u = \begin{cases} e^x & \text{if } x \leq \pi^{-1} \\ e^x + 2x & \text{if } x > \pi^{-1}. \end{cases} \tag{5.3}$$

As both jump conditions are non-homogeneous, we need to extend them in the whole domain Ω. To this aim, we define two possible sets of extension to highlight the role of the choice of the extensions for the convergence of the method. The first set is made of arbitrary functions:

$$\bar{g}_d(x) = -(2\pi^{-1} + \sin(x - \pi^{-1})) \qquad \bar{g}_n(x) = 1 + e^{(x-\pi^{-1})} \tag{5.4}$$

while the second set, called simplified extensions, is made of constant functions:

$$\bar{\bar{g}}_d(x) = -2\pi^{-1} \qquad \bar{\bar{g}}_n(x) = 2 \tag{5.5}$$

For the simplified extensions (5.5), thanks to the definitions (2.10) and (2.13), it is easy to see that the interpolation does not introduce any error while if we take the extensions in (5.4), the interpolation will produce some error on the jumps and the conditions (5.2) will not be satisfied exactly. In the latter case, we have measured the error due to the liftings on the jump conditions (5.2) for $\mathbb{P}_1$ and $\mathbb{P}_2$ finite elements. The following table shows the order of convergence of these errors for $h \to 0$:

	Convergence rates for errors on:			
Elements	$[\![Rg_d]\!]$	$\left[\!\left[\frac{\partial Rg_d}{\partial n}\right]\!\right]$	$[\![Sg_n]\!]$	$\left[\!\left[\frac{\partial Sg_n}{\partial n}\right]\!\right]$
$\mathbb{P}_1$	3	2	2	1
$\mathbb{P}_2$	3	2	3	2

We can see that the orders are optimal for all the quantities and that we have a superconvergence for Rg_d with $\mathbb{P}_1$ elements. This is because of the special circumstance that we are interpolating a function with zero derivative.

We apply now the SESIC method to solve the 1D problem. To measure the associated error, we use three error measures:

- the H^1 norm of the error in the domain $\Omega^* = (0, \pi^{-1} - 0.1) \cup (\pi^{-1} + 0.1, 1)$,
- the L^2 norm of the error in the domain Ω^*,
- the L^∞ norm of the error in the entire domain Ω.

We typically get a quite smooth error pattern on the whole domain, as shown in Fig. 5.1 (left), what provides an evidence that all the components of the error are balanced.

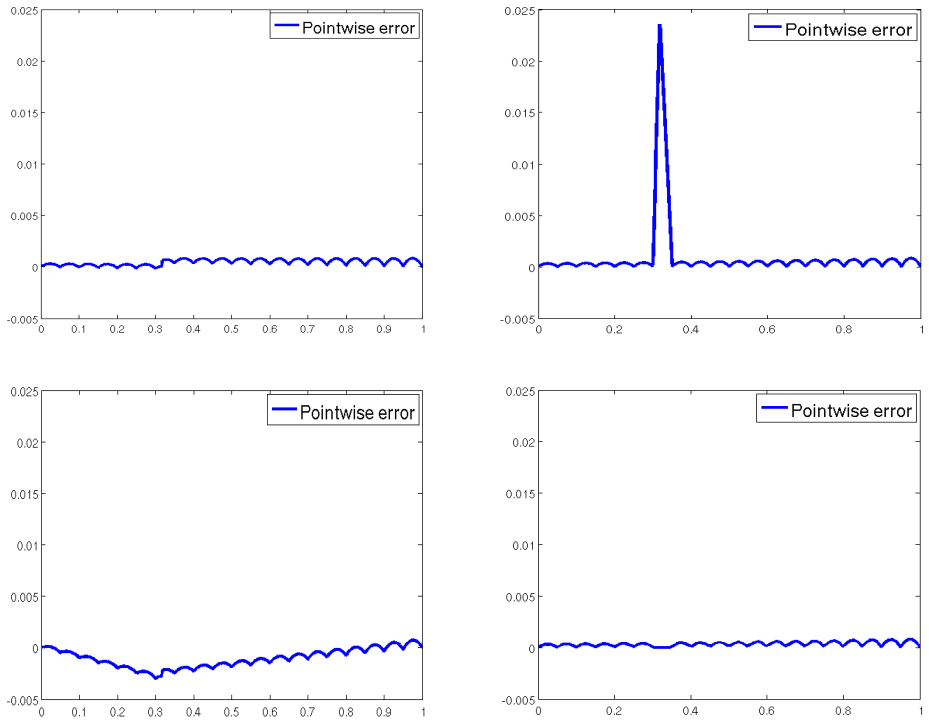

FIG. 5.1. *Pointwise error in the solution for the 1D test using $\mathbb{P}_1$ elements and a grid of* 20 *intervals: top left, using the SESIC method; top right, using the SESIC method without lifting for the normal derivative; bottom left, using the modification* (3.14)*; bottom right, using the ESIC method.*

However, as shown in the next table, we do not get optimal orders for the maximum error with $\mathbb{P}_2$ elements, while the errors in Ω_* and the errors for the $\mathbb{P}_1$ elements exhibit optimal convergence rates:

Norm	$\mathbb{P}_1$ elements	$\mathbb{P}_2$ elements
$L^2(\Omega^*)$	2	3
$H^1(\Omega^*)$	1	2
$L^\infty(\Omega)$	2	*2*

Optimal orders also in the L^∞ norm can be recovered if we use the simplified extensions (5.5). The suboptimality remarked for $\mathbb{P}_2$ might be due to a lack of regularity of $\hat{u}$: we can ensure that $\hat{u} \in H^2(\Omega)$ but we would need to build liftings taking into account also the second derivatives to provide more regularity (See Sect. 3.5).

Using this test case, we can also provide a justification of the use of the lifting for the jump in the normal derivative. If we do not take into account the lifting Sg_n, we have to use the weak formulation (3.2). We keep the same definition for Rg_d (with the extension given in (5.4)).

This produces results that are different from our method mainly near the interface: figure 5.1 (right) shows a large error peak in the element crossed by the interface. The error located in that element is far larger than the interpolation error visible in the other elements.
This additional error comes from the fact that the underlying finite element space cannot reproduce jumps inside the elements. It is then impossible to reduce this error without providing the finite element space with the ability to capture jumps. In the SESIC method, this is the role of the lifting, that carry the jumps but does not belong to the finite element space. We can also see this behavior in the following table that shows the convergence orders for the method without Sg_n: even if the errors computed in the domain Ω_* show optimal convergence orders, the high error near the interface reduces the convergence rates in the maximum norm.

Norm	$\mathbb{P}_1$ elements	$\mathbb{P}_2$ elements
$L^2(\Omega^*)$	2	3
$H^1(\Omega^*)$	1	2
$L^\infty(\Omega)$	*1*	*1*

The role of the lifting Sg_n for the normal derivative is then clear: it helps to reduce the magnitude of the error in the neighborhood of the interface.

For the sake of comparing our method with the ESIC method described in section 3.4, we have also tested the weak formulation modified with (3.14) and with the liftings described in section 3.1. This allows us to bring to light the consequences of using (3.14) (we will use the two-side integration (See Sect. 3.2) to keep the error coming exclusively from method and not from the integration scheme). The following table shows the convergence rates for this test case: we can clearly see that the convergences are slower than with the weak formulation (3.3).

Norm	$\mathbb{P}_1$ elements	$\mathbb{P}_2$ elements
$L^2(\Omega^*)$	*1*	*2*
$H^1(\Omega^*)$	1	2
$L^\infty(\Omega)$	*1*	*2*

Figure 5.1 shows the typical pattern that we get using the modified weak formulation. The solution looks like if the force applied on the interface (by the term $\int_\Gamma g_n v_h$ in (3.2) and (3.3)) was badly estimated, leading to the trend of the error to be greater near the interface, while producing no peak there.
The origin of the error is also emphasized in the next figure, that shows that there is a big correlation between the error $\left| \left[\!\left[\frac{\partial S g_n}{\partial n} \right]\!\right] - g_n \right|$ and the L^2 error.

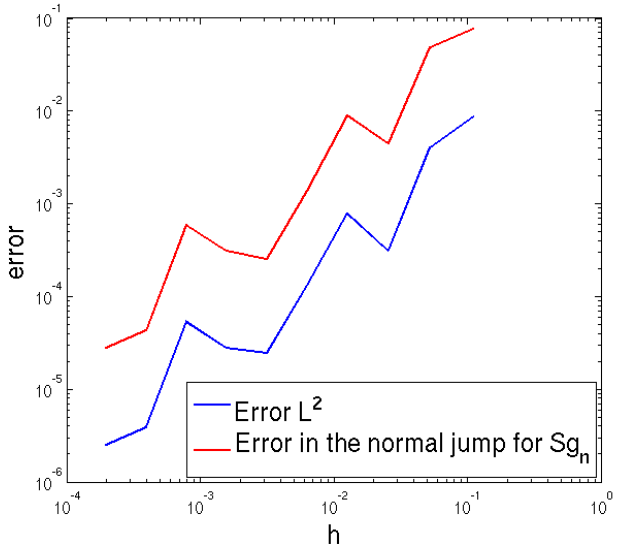

FIG. 5.2. *Comparison between the error on the normal jump of Sg_n and the global L^2 error.*

This error does not show up in the original ESIC method as shown in the next table.

Norm	Convergence rate
$L^2(\Omega^*)$	2
$H^1(\Omega^*)$	1
$L^\infty(\Omega)$	2

The reason is that in the latter method, polynomial refinement is performed near the interface. In this example, $\mathbb{P}_1$ elements have been used except for the elements containing the interface where a $\mathbb{P}_2$ basis was defined. As shown at the beginning of this section, when $\mathbb{P}_2$ are used, the error $|\left[\!\left[\frac{\partial Sg_n}{\partial n}\right]\!\right] - g_n|$ has a second order convergence and then has the same behavior as the interpolation error. However this approach requires an additional programming effort as well as unnecessary addition of degrees of freedom: the next figure shows the pointwise error for the ESIC method and we can observe that the error in the element containing Γ is smaller than in the rest of the domain.

Finally, we investigate the effects of computing integrals using the regularized integrands introduced in section 3.2. We test both widths $w = \sqrt{\frac{h}{2}}$ and $w = h$. The effects of the thickness of the regularization band is clearly visible in Fig. 5.3 (left) where we show the behavior of the $L^2(\Omega^*)$ norm of the error.

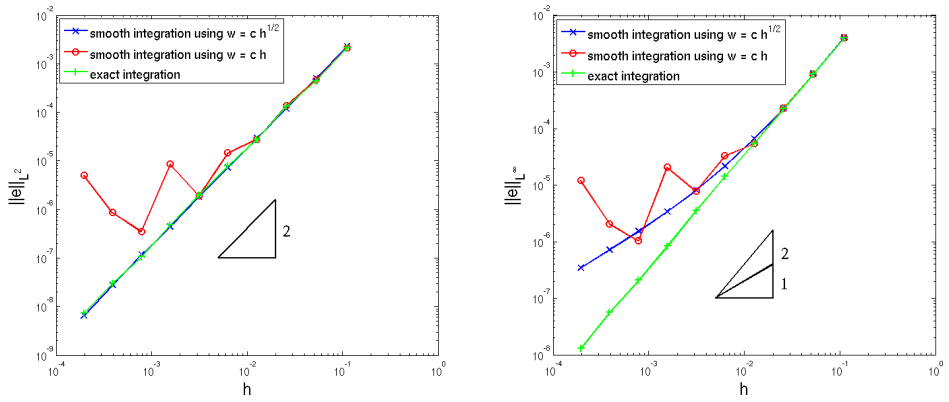

FIG. 5.3. *$L^2(\Omega^*)$ error (left) and $L^\infty(\Omega)$ error (right) associated with the different integration methods.*

As stated previously in this section, optimal order of convergence is achieved with the exact integration. Using the proposed smooth integration, i.e., with w proportional to $\sqrt{h}$, we also get the optimal order of convergence in this norm. On the contrary, using a regularization band with thickness $w = h$, we obtain an unpredictable behavior when h becomes small. The convergence rate in that case is difficult to assess. We can observe the same kind of behavior in the $L^\infty(\Omega)$ norm as shown in Fig. 5.3 (right). In this case we can see that using w proportional to $\sqrt{h}$ leads to a convergence slower than the optimal one: if for coarse meshes the convergence rate seems to be close to 2, it then slows down to 1 for finer meshes.
All these results correspond quite well to the remarks that we made in Sect. 3.2. The smooth integration using w proportional to $\sqrt{h}$ permits to control the error leading to regular convergence, even optimal in the $L^2(\Omega^*)$ norm. This means that the error generated near the interface, reported in the $L^\infty(\Omega)$ norm, is confined in that area and does not pollute the solution in the whole domain. On the contrary, with $w = h$, we lose the control on the quadrature error causing a large error in the interface area that eventually spreads in the whole domain.

5.2. 2D test case. We first test our method on the two dimensional test case defined in [12]. This test is quite simple as the exact solution is continuous, so that the jump is only in the normal derivative. The domain is defined as the square $\Omega = (-1, 1)^2$ and the interface is the circle with radius 0.5 centered at the origin.

The exact solution reads:

$$u(x,y) = \begin{cases} 1 & \text{if } x^2 + y^2 \leq 0.25 \\ 1 - \log(2\sqrt{x^2+y^2}) & \text{if } x^2 + y^2 > 0.25. \end{cases}$$

Dirichlet boundary conditions are set to ensure this exact solution and the jump in the normal derivative to be

$$\left[\!\left[\frac{\partial u}{\partial n}\right]\!\right]_\Gamma = -2.$$

Cartesian meshes with n cells on each side were used. The results that we obtain are listed in the following table:

n	Maximal error on Γ	rate	Maximal error in Ω	rate
9	7.13×10^{-3}		1.84×10^{-2}	
19	2.85×10^{-3}	1.23	4.61×10^{-3}	1.85
39	7.10×10^{-4}	1.93	1.13×10^{-3}	1.96
79	1.71×10^{-4}	2.02	2.71×10^{-4}	2.02

We can see that the SESIC method gives optimal orders of convergence both at the interface and in the entire domain. This means that the error decreases with the same rate everywhere in the domain, included near and on the interface. Moreover, the magnitude of the error is lower than for the methods (ESIC, XFEM and IBM) compared in [12], while being easier to implement and cheaper to compute.

We want then to investigate the influence of the regularity of the interface. The next test case consists in a domain cut by a C^1 curve: the level set function is defined as (see Fig. 5.4 for a representation):

$$\phi(x,y) = \begin{cases} \sqrt{x^2 + (y-0.5)^2} - 0.2 & \text{if } y > 0.5 \\ |x| - 0.2 & \text{if } |y| \leq 0.5 \\ \sqrt{x^2 + (y+0.5)^2} - 0.2 & \text{if } y < -0.5 \end{cases}$$

and the exact solution is defined as

$$u(x,y) = \begin{cases} 1 - \log(2\sqrt{x^2+y^2}) & \text{if } \phi(x,y) \geq 0 \\ 0 & \text{if } \phi(x,y) < 0 \ . \end{cases} \tag{5.6}$$

The Dirichlet boundary conditions on $\partial\Omega$ and the jump conditions across Γ are computed using this exact solution. Using the SESIC method, we obtain the following errors:

n	$H^1(\Omega^*)$ error	rate	$L^2(\Omega^*)$ error	rate	Maximal error in Ω	rate
9	6.63×10^{-1}		4.55×10^{-2}		9.07×10^{-2}	
19	3.23×10^{-1}	0.96	1.19×10^{-2}	1.79	3.50×10^{-2}	1.27
29	2.11×10^{-1}	1.01	5.45×10^{-3}	1.85	1.78×10^{-2}	1.60
39	1.56×10^{-1}	1.01	3.22×10^{-3}	1.78	1.09×10^{-2}	1.64
69	8.85×10^{-2}	1.00	1.12×10^{-3}	1.84	4.07×10^{-3}	1.73
99	6.17×10^{-2}	1.00	6.04×10^{-4}	1.72	2.23×10^{-3}	1.67
149	4.11×10^{-2}	1.00	2.98×10^{-4}	1.73	1.14×10^{-3}	1.65
199	3.08×10^{-2}	1.00	1.85×10^{-4}	1.65	7.13×10^{-4}	1.61

We can remark that the error estimate in H^1 is optimal whereas the errors in the L^2 and L^∞ norms have convergence rates between 1.5 and 2.

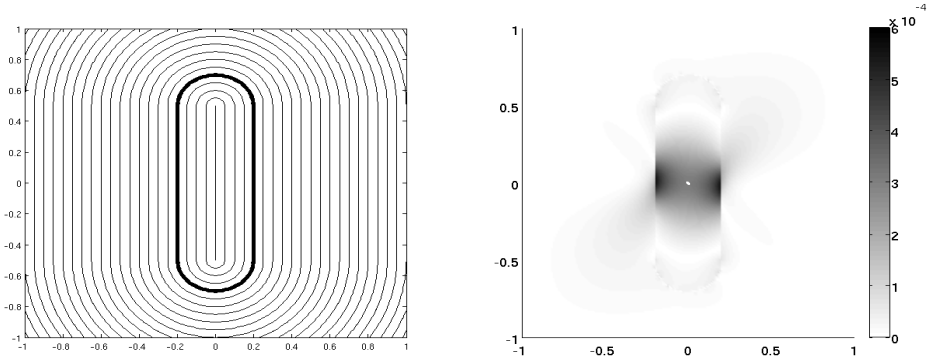

FIG. 5.4. *Representation of the level set function (left,* Γ *bold) and pointwise error produced by the SESIC method with* $n = 99$ *(right).*

Finally, we used the SESIC method to approximate the solution of a problem where the curve Γ is only C^0. We define the level set function as:

$$\phi(x,y) = \begin{cases} \sqrt{(x-\frac{\sqrt{2}}{4})^2+y^2} - 0.5 & \text{if } x \geq 0 \\ \sqrt{(x+\frac{\sqrt{2}}{4})^2+y^2} - 0.5 & \text{if } x < 0 \end{cases}$$

and the exact solution is defined as in (5.6). The next table reports the errors obtained in this test case.

n	$H^1(\Omega^*)$ error	rate	$L^2(\Omega^*)$ error	rate	Maximal error in Ω	rate
9	3.01×10^{-1}		5.26×10^{-2}		7.74×10^{-2}	
19	1.57×10^{-1}	0.87	2.74×10^{-2}	0.88	5.13×10^{-2}	0.55
29	1.04×10^{-1}	0.97	1.86×10^{-2}	0.91	3.48×10^{-2}	0.91
39	7.90×10^{-2}	0.93	1.41×10^{-2}	0.94	2.87×10^{-2}	0.66
69	4.73×10^{-2}	0.90	8.18×10^{-3}	0.96	1.91×10^{-2}	0.71
99	3.40×10^{-2}	0.91	5.68×10^{-3}	1.01	1.47×10^{-2}	0.73
149	2.32×10^{-2}	0.94	3.80×10^{-3}	0.98	1.06×10^{-2}	0.79
199	1.73×10^{-2}	1.01	2.87×10^{-3}	0.98	8.04×10^{-3}	0.97

The lack of regularity of Γ is directly reflected in the convergence orders: the H^1 error as well as those in L^2 and L^∞ norm do not exceed the first order convergence. This can also be seen when looking at the pointwise error (Fig. 5.5) where one can remark that the largest error are created near the two points of low regularity of Γ.

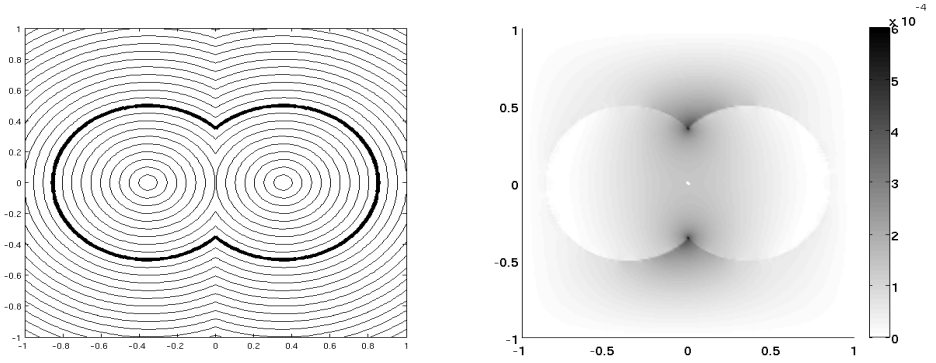

FIG. 5.5. *Representation of the level set function (left,* Γ *bold) and pointwise error produced by the SESIC method with* $n = 99$ *(right).*

5.3. 3D test case. We finally consider a 3D problem. This example was implemented in the parallel version of the finite element library LifeV (www.lifev.org). We consider the domain $\Omega = (-1, 1)^3$. The level set function is $\phi(x, y, z) = \left(x^2 + y^2 + z^2\right)^{1/2} - 0.5$ so that the interface Γ is a sphere centered in the origin with a radius 0.5. In Ω, we want to find the solution $u : \Omega \to \mathbb{R}$ of the problem $-\Delta u = 0$ with jumps conditions through Γ:

$$[\![u]\!]_\Gamma = 2 - e^{x+z}\sin(\sqrt{2}y)$$

$$\left[\!\left[\frac{\partial u}{\partial n}\right]\!\right]_\Gamma = 4 + 2e^{x+z}\left((x+z)\sin(\sqrt{2}y) + \sqrt{2}y\cos(\sqrt{2}y)\right).$$

Boundary conditions are such that the exact solution is

$$u(x, y, z) = \begin{cases} (x^2 + y^2 + z^2)^{-1/2} & \text{if } \phi(x, y, z) \geq 0 \\ e^{x+z}\sin(\sqrt{2}y) & \text{if } \phi(x, y, z) < 0. \end{cases}$$

We solved this problem using $\mathbb{P}_1$ finite elements. To measure the error, we computed both the L^2 error in the domain $\Omega^* = \{\mathbf{x} \in \Omega \mid |\phi(\mathbf{x})| > 0.1\}$ for regularity and maximal error in all the finite element nodes (denoted hereafter l^∞). We used Cartesian meshes with n representing the number of nodes in each direction. The computed errors and convergence rates are given in the next table.

n	degrees of freedom	error $L^2(\Omega^*)$	rate	error l^∞	rate
5	125	6.26×10^{-1}		3.52×10^{-1}	
10	1000	2.11×10^{-1}	1.34	8.39×10^{-2}	1.79
20	8000	1.72×10^{-2}	3.36	2.09×10^{-2}	1.86
40	64000	3.07×10^{-3}	2.40	5.63×10^{-3}	1.82
60	216000	1.34×10^{-3}	2.00	2.63×10^{-3}	1.84
80	512000	7.50×10^{-4}	1.99	1.67×10^{-3}	1.56
100	1000000	4.78×10^{-4}	2.00	1.17×10^{-3}	1.58

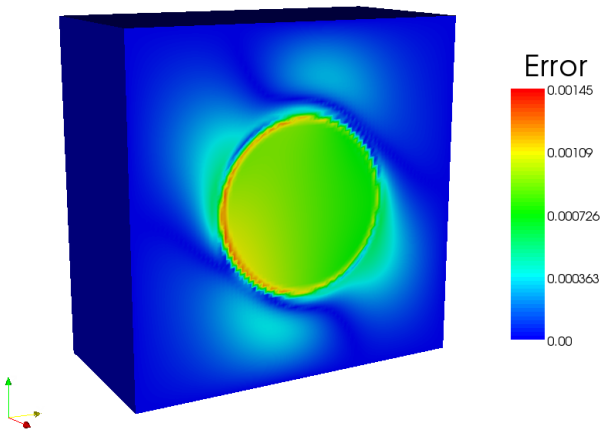

FIG. 5.6. *Representation of the error on the surface $x = 0$ for $n = 80$. We can remark that the error near the interface is of the same order of magnitude as far from it.*

The order of convergence in the $L_2(\Omega^*)$ norm is close to the optimal rate 2 when n increases. This is due to the fact that the error produced by the smooth integration is well controlled and it is reflected only in the l^∞ norm as it is confined to the interface area (as shown in Fig. 5.6). The error in the l^∞ norm is expected to behave like the $L^\infty(\Omega)$ error in the 1D test case, i.e., to decrease slowly for finer meshes until it reaches the convergence rate 1.

Finally, with this test case we can emphasize the need for a good integration scheme for the singular functions. Indeed, if instead of smoothing the integrands on a width proportional to $\sqrt{h}$, we use a width of h, we get the following results:

n	degrees of freedom	error $L^2(\Omega^*)$	rate	error l^∞	rate
5	125	6.33×10^{-1}		3.18×10^{-1}	
10	1000	2.16×10^{-1}	1.33	7.23×10^{-2}	1.83
20	8000	1.71×10^{-2}	3.39	1.86×10^{-2}	1.82
40	64000	3.92×10^{-3}	2.05	1.27×10^{-2}	0.53
60	216000	1.38×10^{-3}	2.52	5.47×10^{-3}	2.03
80	512000	1.17×10^{-3}	0.57	7.57×10^{-3}	−1.11
100	1000000	1.01×10^{-3}	0.65	5.82×10^{-3}	1.16

We can observe that the convergence is slower when the mesh gets finer because the quadrature error is dominating.

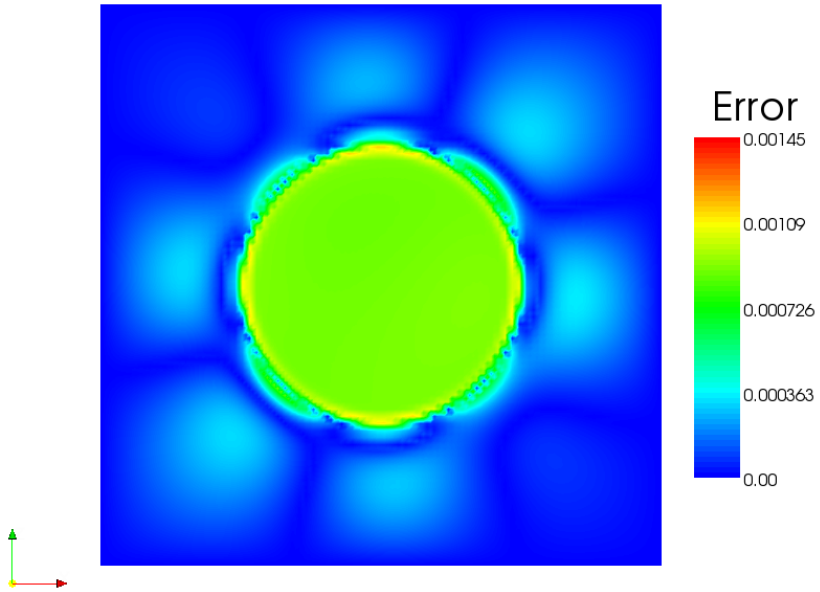

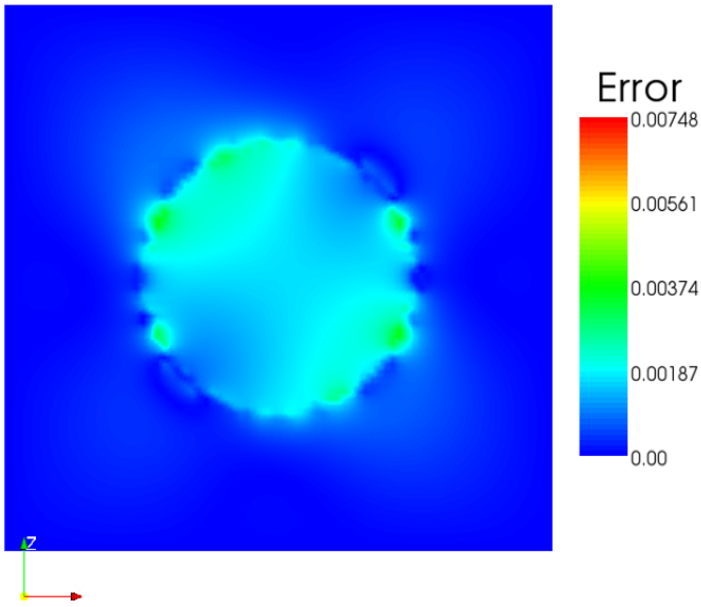

FIG. 5.7. *Error for the 3D test case on the plane $y = 0$. The upper figure represents the error when the interface width is $w = 0.0796$ $(= \sqrt{h/2})$, whereas for the lower figure we used $w = 0.0127$ $(= h)$.*

6. Conclusions. In this paper, we have investigated a new method, the SESIC method, that can be used to solve interior discontinuity interface problems. It relies on simple construction of liftings, i.e. finite element functions that are built to carry the discontinuities across the interface.

The method that we proposed was inspired by the ESIC method (see [12]) and in fact inherits some properties of that method. First of all, the jumps across the interface are actually reproduced by the method. The cost for this method is also quite low, as only the assembly for a small part (corresponding to the elements crossed by the interface) of the right hand side is needed.

The SESIC method has also the advantage of requiring no additional degree of freedom, as no new basis function nor refinement near the interface are necessary. The consequence is that the stiffness matrix remains unchanged with respect to that associated with the given PDE without interface discontinuities. At the algebraic level, solution strategies and preconditioning need not be modified. The liftings introduced in the SESIC method have removed one of the bottlenecks of the ESIC method: there is no need to reconstruct the interface explicitly for building the liftings. This adds more generality to the method, as the level set can now be given in all the possible forms: even a level set given as a finite element function with high polynomial degree would be acceptable, as there is no need to solve a non-linear equation for finding the zero level set. Moreover, if we use regularizing functions for the integration of discontinuous integrands, then the SESIC method treats the interface in a fully implicit way.

The numerical results show that in the 1D and 2D cases that we have tested, the method exhibits optimal orders of convergence. The use of regularized integrands rather than exact integration across the interface leads to a slower convergence in the regularization band around the interface, but it keeps the optimal convergence in the remaining part of the domain, as shown on the 3D test case that we have considered.

Future work will focus on the use of this method in much more complicated problems, in particular free surface flows. Indeed, in the latter case, jumps can appear across the interface, for example in the pressure when surface tension acts on the interface or in the gradient of the pressure when gravity is considered. A paper showing how to apply the SESIC method to improve the accuracy of such simulations is in preparation.

Acknowledgements. The authors acknowledge the support of the Swiss National Science Foundation, Project Sinergia 125444: "Fluid dynamics and mixing behavior in orbitally shaken bioreactors for mammalian cell cultivation". We would like to acknowledge professors J. Sethian and J.-S. Huh for many useful comments on an earlier version of this paper.

REFERENCES

[1] R.A. Adams. *Sobolev spaces*. Pure and Applied Mathematics - Academic. Academic Press, 1975.

[2] P.M.A. Areias and T. Belytschko. Analysis of three-dimensional crack initiation and propagation using the extended finite element method. *Internat. J. Numer. Methods Engrg.*, 63:760–788, 2005.

[3] E. Béchet, H. Minnebo, N. Moës, and B. Burgardt. Improved implementation and robustness study of the X-FEM for stress analysis around cracks. *Internat. J. Numer. Methods Engrg.*, 64:1033–1056, 2005.

[4] J. Bedrossian, J.H. von Brecht, S. Zhu, E. Sifakis, and J. M. Teran. A second order virtual node method for elliptic problems with interfaces and irregular domains. *J. Comput. Phys.*, 229(18):6405–6426, 2010.

[5] T. Belytschko, N. Moes, S. Usui, and C. Parimi. Arbitrary discontinuities in finite elements. *Internat. J. Numer. Meth. Engng.*, 50:993–1013, 2001.

[6] S. Brenner and R. Scott. *The mathematical theory of finite element methods*. Springer, 2008.

[7] G. Caginalp and X. Chen. Phase field equations in the singular limit of sharp interface problems. In *On the Evolution of Phase Boundaries (Minneapolis, MN, 1990–91)*, volume 43 of *IMA Vol. Math. Appl.*, pages 1–27. Springer, New York, 1992.

[8] J. Chessa, P. Smolinski, and T. Belytschko. The extended finite element method (XFEM) for solidification problems. *Internat. J. Numer. Methods Engrg.*, 53:1959–1977, 2002.

[9] D.A. Dunavant. High degree efficient symmetrical gaussian quadrature rules for the triangle. *Internat. J. Numer. Methods Engrg.*, 21:1129–1148, 1985.

[10] S. Gross and A. Reusken. An extended pressure finite element space for two-phase incompressible flows with surface tension. *J. Comput. Phys.*, 224(1):40–58, 08 2007.

[11] P. Hansbo. Nitsche's method for interface problems in computational mechanics. *GAMM-Mitt*, 28(2):183–206, 2005.

[12] J.-S. Huh and J.A. Sethian. Exact subgrid interface correction schemes for elliptic interface problems. *Proceedings of the National Academy of Sciences of the United States of America*, 105(29):9874, 2008.

[13] B.L. Vaughan Jr, B.G. Smith, and D.L. Chopp. A comparison of the extended finite element method with the immersed interface method for elliptic equations with discontinuous coefficients and singular sources. *Comm. Appl. Math. Comp. Sci.*, 1:207–228, 2006.

[14] Z. Li and M.-C. Lai. The immersed interface method for the NavierStokes equations with singular forces. *J. Comput. Phys.*, 171(2):822–842, 08 2001.

[15] J.L. Lions and E. Magenes. *Non-homogeneous boundary value problems and applications*. Springer, 1972.

[16] D.Q. Nguyen, R.P. Fedkiw, and M. Kang. A boundary condition capturing method for incompressible flame discontinuities. *J. Comput. Phys.*, 172:71–98, 2000.

[17] S. Osher and R.P. Fedkiw. *Level Set Methods and Dynamic Implicit Surfaces*. Springer, 2002.

[18] N. Parolini. *Computational Fluid Dynamics for Naval Engineering Problems*. PhD thesis, Ecole Polytechnique Fédérale de Lausanne, 2004.

[19] Danping Peng, Barry Merriman, Stanley Osher, Hongkai Zhao, and Myungjoo Kang. A pde-based fast local level set method. *Journal of Computational Physics*, 155(2):410 – 438, 1999.

[20] A. Quarteroni. *Numerical Models for Differential Problems*. Springer, 2009.

[21] A. Quarteroni, R. Sacco, and F. Saleri. *Numerical mathematics*. Springer, 2007.

[22] A. Quarteroni and A. Valli. *Numerical Approximation of Partial Differential Equations*. Springer, Berlin, 1994.

[23] Ridgway Scott. Interpolated boundary conditions in the finite element method. *SIAM Journal on Numerical Analysis*, 12(3):pp. 404–427, 1975.

[24] J. A. Sethian. *Level Set Methods and Fast Marching Methods*. Cambridge University Press, Cambridge, second edition, 1999.

[25] A.K. Tornberg. Multi-dimensional quadrature of singular and discontinuous functions. *BIT Numerical Mathematics*, 42(3):644–669, 2002.

Recent publications :

MATHEMATICS INSTITUTE OF COMPUTATIONAL SCIENCE AND ENGINEERING
Section of Mathematics
Ecole Polytechnique Fédérale
CH-1015 Lausanne

18.2010 M. DISCACCIATI, A. QUARTERONI, S. QUINODOZ:
Numerical approximation of internal discontinuity interface problems

19.2010 B. KALTENBACHER, M. KALTENBACHER, I. SIM:
Perfectly matched layer technique for the second order wave equations in time domain

20.2010 T. LASSILA, G. ROZZA:
Model reduction of semiaffinely parameterized partial differential equations by two-level affine approximation

21.2010 T. HOFER, J. RAPPAZ:
Numerical conservation schemes for convection-diffusion equations

22.2010 G. ROZZA, D.B. PHUONG HUYNH, A. MANZONI:
Reduced basis approximation and a posteriori error estimation for Stokes flows in parametrized geometries : roles of the inf-sup stability constants

01.2011 T. LASSILA, A. QUARTERONI, G. ROZZA:
A reduced basis model with parametric coupling for fluid-structure interaction problems

02.2011 A. QUARTERONI, G. ROZZA, A. MANZONI:
Certified Reduced Basis Approximation for Parametrized Partial Differential Equations and Applications

03.2011 M. LOMBARDI, N. PAROLINI, A.QUARTERONI, G. ROZZA:
Numerical simulation of sailing boats: dynamics, FSI and shape optimization

04.2011 P. BLANCO, P. GERVASIO, A. QUARTERONI:
Extendet variational formulation for heterogeneous partial differential equations

05.2011 A. MANZONI, A. QUARTERONI, G. ROZZA:
Model reduction techniques for fast blood flow simulation in parametrized geometries

06.2011 M. ASTORINO, J. BECERRA SAGREDO, A. QUARTERONI:
A modular lattice Boltzmann solver for GPU computing processors

07.2011 L. IAPICHINO, A. QUARTERONI, G. ROZZA:
A reduced basis hybrid method for the coupling of parametrized domains represented by fluidic networks

08.2011 T. LASSILA, A. MANZONI, G. ROZZA:
On the approximation of stability factors for general parametrized partial differential equations with a tow-level affine decomposition

09.2011 M. DISCACCIATI, A. QUARTERONI, S. QUINODOZ:
Numerical approximation of internal discontinuity interface problems